0273-2289/96/6003—0251$17.75

On the Topological Features of Optimal Metabolic Pathway Regimes

SHEAU MIN SEE, JON P. DEAN, AND GEORGE DERVAKOS*

Department of Chemical Engineering, University of Manchester Institute of Science and Technology, P. O. Box 88, Manchester, M60 1QD, UK

Received April 12, 1995; Accepted August 21, 1995

ABSTRACT

In this work, the stoichiometric metabolic network of *Escherichia coli* has been formulated as a comprehensive mathematical programming model, with a view to identifying the optimal redirection of metabolic fluxes so that the yield of particular metabolites is maximized. Computation and analysis has shown that the over-production of a given metabolite at various cell growth rates is only possible for a finite ordered set of metabolic structures which, in addition, are metabolite-specific. Each regime has distinct topological features, although the actual flux values differ. Application of the model to the production of 20 amino acids on four carbon sources (glucose, glycerol, lactate, and citrate) has also indicated that, for fixed cell composition, the maximum amino acid yield decreases linearly with increasing cell growth rate. However, when the cell composition varies with cell growth rate, the amino-acid yield varies in a nonlinear manner. Medium optimization studies have also demonstrated that, of the above substrates, glucose and glycerol are the most efficient from the energetic viewpoint. Finally, model predictions are analyzed in the light of experimental data.

Index Entries: *Escherichia coli*; metabolic engineering; linear programming; amino acids.

*Author to whom all correspondence and reprint requests should be addressed.

General Nomenclature: b, vector of net conversion rates, T^{-1}; C, time required to replicate the chromosome, T; C_p, peptide elongation rate, LT^{-1}; D, time period between termination of a round of replication and the following cell division, T; D_i, drain factor of metabolite, i, T^{-1}; $(D_s/r_x)_{gr}$, growth related dissipation of Gibbs energy, L^2T^{-2}; f_{ai}, amount of amino acid, ai, needed for biomass formation, M; J_i, reaction flux, T^{-1}; m_e, maintenance related dissipation of Gibbs energy, L^2T^{-2}; P, total protein in cell, M; P_o, protein per origin, M; S, stoichiometric matrix; t, time, T; X, metabolite concentration, ML^{-3}; $Y_{ATP/X}$, biomass yield coefficient; Z, objective function, T^{-1}.

Greek Symbols: α_i, maximum flux allowable through reaction flux, v_i, T^{-1}; β_r, ribosome activity; μ, specific growth rate, T^{-1};τ, doubling time, T; ν, vector of net conversion rates, T^{-1}; ν_i, flux of reaction i, T^{-1}; γ_s, degree of reduction; γ_{ai}, amount of amino acid over the total amino acid in cell.

INTRODUCTION

Few, if any, biochemical processes achieve economic viability by using natural isolates of microorganisms. Instead, a long and, usually, empirical process has to be gone through to improve product yields. This is, however, an inefficient method, especially when the metabolic regulatory systems oppose the desired changes. In recent years, the focus has been on metabolic engineering, which is the purposeful modification of intermediary metabolism using recombinant DNA techniques, to produce such mutants. Some possible applications of metabolic engineering include: the improvement of the production of chemicals already produced by the host organism; the extension of the substrate range for growth and production formation; the addition of new catabolic activities for degradation of toxic chemicals; and the production of chemicals new to the host organism. By cloning and expressing multiple genes in the host organism and altering its regulatory properties at the genetic and enzymatic levels, increased levels of production of various metabolites have been obtained. These include tyrosin (*1*), phenylalanine (*2*), ethanol (*3,4*), tylosin (*5*) and cephamycin C (*6*). More important perhaps is the production of new antibiotics such as spiramycin (*7*) and polymers such as polyhydroxytbutyrate (PHB) (*8*). A very practical aspect of metabolic engineering is the extension of the substrate range that a host organism can use for growth and product formation. Most of the work has been focused on engineering organisms to use lactose, a major by-product in the cheese-making industry and xylose (*9*).

Metabolic engineering draws on a wide range of disciplines and technologies in order to successfully engineer a cell or organism. One important class of tools used in metabolic engineering is mathematical tools which assist in modeling, designing, and predicting the properties of

modified organisms. A case in point is the development of tools to characterize the dynamic behavior of cells. Several attempts have been made to systematically model metabolic dynamics (*10,11*) but progress appears to have been hampered by the lack of kinetic and regulatory information on the function of all the enzymes in a particular cell. Recently, however, Shiraishi and Savageau (*12–16*), in a series of papers, presented a complete kinetic model for the tricarboxylic acid cycle of *Dictyostelium discoideum.*

Despite its obvious limitations, optimization based entirely on stoichiometric information can be a valuable tool in interpreting the behavior of complex metabolic pathway structures. This has already been demonstrated by several researchers. The application of linear programming methods to elucidate the regulation of triacylglycerol synthesis from glucose in rat adipocytes was investigated by Fell and Small (*17*). In another study (*18*), the stoichiometry of the main pathways in *Escherichia coli* was employed in order to explain the overproduction of acetate in aerobically grown strains. In a series of papers, Papoutsakis and coworkers demonstrated the relevance of using stoichiometric information by deriving a fermentation equation capable of calculating maximum metabolite yields and selectivities for products involved in mixed-acid fermentations (*19–21*). Expanding these ideas, Tsai and Lee (*22*) applied the Gibb's rule of stoichiometry and managed to reduce the size of the system of equations, deriving a simpler equation more practical for on-line monitoring.

An attempt to present a systematic formalism for the stoichiometric analysis of metabolic networks has been presented by Noorman *et al.* (*23*) who introduced three tests—the independancy, consistency, and observability tests—to ensure a correct stoichiometric description of metabolic structures. In a series of papers, Palsson and coworkers applied linear programming to a number of systems including a hybridoma cell line (*25,26*), the main catabolic pathways of *E. coli* (*27*), the flux distributions for optimal production of 20 amino acids and 4 nucleotides (*28*), and the production patterns of *E. coli* under different oxygenation conditions (*29*). Finally, Stephanopoulos and Vallino (*30*) introduced the concept of network rigidity to identify the critical branch points in the overall flux distribution and applied the technique to explain the suboptimal yield of lysine in continuous culture (*31*).

The goal of this work is to analyze cell behavior using entirely stoichiometric information and to identify the topological features of pathway regimes which result in optimal metabolite production. Linear programming is used to examine the biosynthetic capabilities of the bacterium, *Escherichia coli* and assess the relative importance of product formation and cell growth. The approach used in this study is to formulate mass balances for each major metabolite in the cell and then calculate the steady-state flux through each pathway. Through this work, we also seek to determine the optimum pathway utilization and maximum yields of each of the 20 amino acids on various substrates.

Table 1
The Catabolic and Anabolic Pathways of *E. coli* Considered in this Model

a)	Glycolysis
b)	Gluconeogenesis
c)	Pentose phosphate shunt (PPS)
d)	Electron transport system (ETS)
e)	Tricarboxylic acid (TCA) cycle
f)	Amino acid pathways
g)	Biomass formation

MODEL DEVELOPMENT

Theoretical metabolic pathway models have the potential to assist bioprocess development by identifying metabolic regimes and pathway structures which should result in maximizing the yield of the metabolite of interest. The information obtained from such models can then be used to genetically engineer cells so that they can meet the desired level of biological production.

Selection of the host organism in such studies is very important. In this work *E. coli* has been selected as the model biological system for a number of reasons. First of all, *E. coli* is well documented in comparison with other micro-organisms and information regarding its metabolic system is readily available. Secondly, cloning vectors are available for *E. coli*, thus facilitating the use of recombinant DNA techniques to construct the "ideal" organism for the bioprocess. Thirdly, *E. coli* has been known to grow on a wide range of substrates and its ability to utilize inexpensive sources of nutritional supplements may enable the design of low-cost media. Finally, many organisms have been shown to have similar metabolic systems to *E. coli*. This, in turn, enables information obtained on *E. coli* to be applied to predict the behavior of other biological systems.

There are hundreds of enzymatic reactions that occur in *E. coli*. In this model, only the key reactions which play an important role in the major pathways have been selected, and this amounts to approximately 200 reactions. The major catabolic and anabolic pathways underlying this model are summarized in Table 1.

The *E. coli* model presented in this work is based solely on stoichiometry. This method has the advantage in that it does not require kinetic data or other regulatory information, as it is based entirely on the stoichiometry of the reaction network and the metabolic demands placed upon it. In addition, and perhaps more importantly, one can investigate to what extent the metabolic system is limited by stoichiometry only. Once this information is obtained, one may infer the relative contributions of stoichiometric limitations and biological reaction kinetic limitations to the overall system.

The general equation that describes the mass balances of the compounds participating in intermediary metabolism is given by:

$$dX / dt = S \cdot v - b \tag{1}$$

where X is the vector of metabolite amounts per cell, S is the nxm stoichiometric matrix, n is the number of metabolites, v is the vector of m reaction fluxes, and b is the net output from cellular metabolism. The element S_{ij}, is the stoichiometric coefficient of the i_{th} compound in the j_{th} reaction. Assuming that the rate of volume expansion due to cell growth is insignificant in comparison to metabolic transients and that the rate of synthesis of intermediates and macromolecules is constant throughout the growth cycle, then the above equation is simplified into its steady state form:

$$S \cdot v = b \tag{2}$$

The stoichiometric matrix used in this study is based, largely, on two stoichiometric models published by Varma et al. (*28,29*) and Varma and Palsson (*27*) which describes, respectively, the catabolic and the biosynthetic pathways of *E. coli*. The full complement of the metabolic reactions is presented in Appendix A.

The reaction network of *E. coli* represented by the metabolic system sums up to a total of 120 metabolites and 163 reaction fluxes. Assuming that the essence of any metabolic model would be to identify values for these reaction fluxes, one is left with 120 possible mass balances and 163 unknowns. The *E. coli* model is thus under-determined, i.e., there are more variables than equations. Consequently, the stoichiometry of the metabolic network on its own cannot force a unique steady state condition of the metabolic network, leading to an infinite number of possible flux distributions. In this work, the selection of the optimum flux distribution has been achieved by formulating the system using the mathematical programming formalism. This is done by formulating what is known as the "*objective function*" which is a solution that maximizes or minimizes some linear combination of fluxes. The mathematical formulation for the objective function, Z, is:

$$maximize\ Z = \Sigma\, c_i v_i \tag{3}$$

where Z is the objective function represented as a linear combination of the fluxes v_i and c_i is the stoichiometric coefficient of the flux v_i.

The model variables are reaction fluxes and are normalized with regard to biomass (mmol·g^{-1}DW·h^{-1}). The drain flux to biomass is expressed in g biomass formed per g biomass per hour; it represents the growth rate of *E. coli*, μ (h^{-1}). By fixing the glucose uptake rate to 10 mmol·g^{-1} DW·h^{-1}, different levels of production of amino acid can be obtained at different cell growth rates.

In the present work, the maximization of the yields of the 20 amino acids has been chosen as the objective function. This function simply consists of the sum of all the fluxes that consume and produce the amino acid

in question in the network. To maximize the production of an amino acid,the reaction fluxes leading to its production must be optimized. For example, to maximize L-lysine (*Lys*) production, the following reaction which produces *Lys*, is of immediate concern:

$$\text{mDAP} \rightarrow \textbf{Lys} + CO_2 \qquad \text{(Reac. No. 73)}$$

In order to signify that the objective function is to maximize *Lys* production, one has to introduce a separate variable (D_i) into the flux balance equation of *Lys* (Eq. 4) to represent the amount of metabolite that leaves the system. In other words, this variable is the objective function of the optimization.

$$Lys = \mathbf{J('73')} - 0.32\mu - D_i \tag{4}$$

The term 0.32μ represents the amount of *Lys* needed for biomass formation. The optimization of the mathematical model is subject to the following constraints:

$$S \cdot v = b \tag{5}$$

$$v_i \leq \alpha_i,\ i = 1,2,\ldots,m \tag{6}$$

$$v_i \geq 0 \tag{7}$$

The first set of constraints is simply the matrix equation from Equation 2. The second set of constraints represents the maximum values allowable, α_i, for the reaction fluxes v_i. This constraint recognizes the fact that fluxes through individual enzymatic reactions are limited by the amount of enzyme present in the cell, as well as by the rate with which that particular enzyme can react with the substrate. The actual values of the limits (α_i) may be estimated from experimental measurements. In this model, α_i is set to infinity to prevent any reaction limitation of the metabolic system. Constraints included in the model can be divided into *equality* and *inequality* constraints. The flux balance equations constitute the equality constraints and the restriction of fluxes to positive values only gives the inequality constraints. Some equality constraints such as the biomass and cofactor equations are clearly of greater importance. Hence, more emphasis will be given to these equations in later sections.

The biomass equation has been formulated as a drain on the various metabolites produced in the system according to the cellular composition of *E. coli* (Table 2).

In this model, there is no glycogen in the metabolite list. This is because glycogen is not normally formed during cell growth. It is formed when cells are not growing and there is excess glucose present. Instead of glycogen, a drain of *ADP-Glc*, an intermediate in the glycolytic pathway, to biomass has been defined in the *E. coli* model (Eq. 8).

$$G1P + ATP \rightarrow ADPGlc + PPi \tag{8}$$

Table 2
Chemical Composition of *E. coli* Used to Define the Drain Fluxes for Biomass Formation (*44,45*).
All the Demands are in mmol·g^{-1} Dry Weight (DW)

Residues	Amt. (μmol·g^{-1} DW)	Residues	Amt. (μmol·g^{-1} DW)	Residues	Amt. (μmol·g^{-1} DW)
Amino acids		*RNA nucloetides*		*Lipid Components*	
Alanine	488	AMP	165	Glycerol	161
Arginine	281	GMP	203	Ethanolamine	97
Asparagine	229	CMP	126	$C_{16:0}$ fatty acid (43%)	
Aspartate	229	UMP	136	$C_{16:1}$ fatty acid (33%)	
Cysteine	87			$C_{18:1}$ fatty acid (24%)	
Glutamate	250	*DNA nucleotides*		Average fatty acid	258
Glutamine	250	dAMP	24.5		
Glycine	582	dGMP	25.4	*LPS components*	
Histidine	90	dCMP	25.4	Glucose	16.8
Isoleucine	276	dTMP	24.6	Glucosamine	16.8
Leucine	428			Ethanolamine	25.2
Lysine	326	*Peptidoglycan components*		Rhamnose	8.4
Methionine	146	N-Acetylglucosamine	27.6	Heptose	25.2
Phenylalanine	176	N-Acetylmuramic acid	27.6	KDO	25.2
Proline	210	Alanine	55.2	Hydroxymyristic acid	33.6
Serine	205	Diaminopimelate	27.6	Fatty acid ($C_{14:0}$)	16.8
Threonine	241	Glutamate	27.6		
Tryptophan	54			*Polyamines*	
Tyrosine	131	Glycogen	154	Putrescine	34.1
Valine	402			Spermidine	7

It is well-known that the composition of *E. coli* varies with cell growth rate. It was first demonstrated by Schaechter et al. in 1958, (*32*), that the macromolecular composition of the bacterial cell is related to its metabolic activity. The major findings from this work are:

1. Fast-growing bacteria are larger and contain more DNA, RNA, and protein than slow-growing bacteria.
2. The amounts of these macromolecules are exponential functions of cell growth rate.
3. The exponents of these functions are different for different macromolecules.

Bremer and Dennis (*33*) demonstrated that for a given temperature, RNA and ribosome concentrations increase with increasing cell growth rate, DNA concentration decreases, and protein concentration remains almost constant.

Various equations have been proposed in the literature to describe the macromolecular composition of a cell in an exponential culture (*34–36*). Macromolecular composition can be expressed as a function of the culture doubling time τ, and five additional parameters: C (the time required to replicate the chromosome), D (the time period between termination of a round of replication and the following cell division), P_o (protein per origin), β_r (ribosome activity), and C_p (rate of peptide chain elongation rate). Protein per origin is the ratio of protein per genome and origins per genome where the origin represents *oriC* at 84 min on the *E. coli* genetic map. β_r is the fraction of total ribosomes actively engaged in peptide chain elongation.

Despite the availability of models in the literature which relate cell composition to the cell growth rate, all the previous work on the *E. coli* metabolic network appears to have been based on fixed cell composition (*27,28*). In this present study, the varying composition of *E. coli* has been taken into account in the mathematical model. This has included 28 of the 37 components making up biomass. The remaining 9 components of biomass were assumed to be constant and independent of cell growth rate. This includes fatty acids for which no equation could be found in the literature relating fatty acid composition to the cell growth rate. Since lipids only constitute a small proportion of the cell composition, the relative error was deemed to be insignificant.

The biomass equation for the model (Eq. 9) has been formulated as shown:

$$\begin{aligned} 45.13\,ATP + f_{a1}\,Gly + 0.04\,MTHF + f_{a2}\,Glu + f_{a3}\,Gln + f_{a4}\,Phe + f_{a5}\,Tyr + f_{a6}\,Ser + f_{a7}\,Trp + f_{a8}\,Asp + f_{a9}\,Asn + f_{a10}\,Lys + f_{a11}\,Cys + f_{a12}\,Met + f_{a13}\,Thr + f_{a14}\,Ile + f_{a15}\,Pro + f_{a16}\,Arg + f_{a17}\,Ala + f_{a18}\,Val + f_{a19}\,Leu + f_{a20}\,His + f_{r2}\,GTP + f_{r3}\,UTP + f_{r4}\,CTP + f_{d1}\,dATP + f_{d2}\,dGTP + f_{d3}\,dCTP + f_{d4}\,dTTP + 0.09\,PE + 0.02\,PG + 0.02\,CL + 0.154\,ADPGlc \\ + 0.01\,LPS + 0.02\,Peptide + 0.05\,PTRSC + 0.01\,SPRMD \\ \rightarrow Biomass + 44.96\,ADP + 44.96\,Pi \end{aligned} \quad (9)$$

Table 3
Equations Relating the Cell Composition
in Exponential Cultures to Basic Cell Cycle Parameters

Parameter	Symbol	Equation
Protein/cell	P	$P = P_o 2^{(C + D)/\tau}$
RNA/cell	R	$R = K'(P_o/c_p)(1/\tau)2^{(C + D)/\tau}$
		$K' =$ (nucleotides/ribosome)·1n2/[f_s·(1 − f)·β_r·60]
		f_s = fraction of total RNA that is stable RNA
		f_t = fraction of stable RNA that is tRNA
DNA/cell	G	$G = [\tau/(C \cdot \ln 2)][2^{(C + D)/\tau} - 2^{D/\tau}]$
Peptide chain elongation	c_p	$c_p = K'/(R/P)\tau$

Where f_{ai},f_{ri}, and f_{di} are the amounts of amino acid, RNA and DNA needed for biomass formation (mmol·g^{-1} DW). Refer to Appendix A for the abbreviations of the biomass components. f_{ai} can be calculated as follows:

$$f_{ai} = \gamma_{ai} P / 100 \quad (10)$$

$$P = P_o 2^{(C + D)/\tau} * 5.95E\text{-}9 \quad (11)$$

Where γ_{ai} is the percentage of amino acid *ai* directed toward biomass formation (obtained from Table 2), P is the total protein in the cell (mmol·g^{-1} DW) P_o is the protein per origin (aa residues), $2^{(C + D)/\tau}$ is the number of origins per cell (no.cell^{-1}), τ is the doubling time (min), C is the time required to replicate the chromosome (min) and D is the time period between termination of a round of replication and the following cell division (min). The value of *5.95E-9* in Equation 11 is a conversion factor for converting the units of total protein from aa residues per cell of protein to *mmol* of protein per *g* DW. Values for P_o, C, and D have been determined experimentally at various cell growth rates (33). The amounts of RNA and DNA required for biomass formation are calculated using a similar procedure and the equations given in Table 3.

Various types of cofactors are included in the metabolic model, some more important than others. Quite clearly, *ATP, NADH,* and *NADPH* are key cofactors providing the tie between the various biosynthetic pathways. An indicator of the "relative" importance of these cofactors is the number of reactions that these metabolites are involved in. The stoichiometric matrix of *E. coli* is rather "sparse", i.e., most metabolites are only involved in just a few reactions. However, cofactors are involved in many reactions. For example, in this model there are 6 reactions that produce *ATP* and 46 reactions that consume it. From the large number of reactions that involve *ATP*, it can be seen that *ATP* plays a very important role in regulating metabolism.

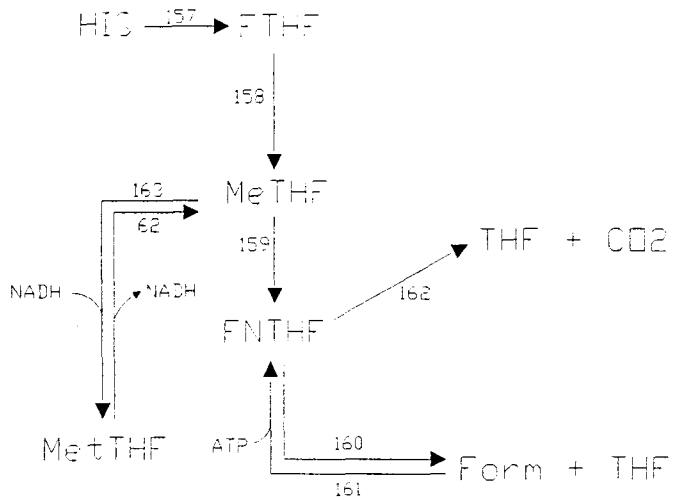

Fig. 1. Production/consumption of cofactors.

Literature values of the amount of *ATP* needed for biomass synthesis in *E. coli* range from 45.13 mmol·g^{-1} DW·h^{-1} (*28,29*) to 117 mmol·g^{-1} DW·h^{-1} (*37*). This indicates the uncertainity over the amount of *ATP* required for biomass formation. In view of this disparity, these two values have been used to define the upper and lower limits for *ATP* demand. Hence, instead of a unique yield of amino acid at a specified cell growth rate, a range of yields may be obtained, depending on the actual *ATP* needed for biosynthesis.

Besides *ATP*, *NADH*, and *NADPH*, several other cofactors are also involved in metabolite formation. In the present study, an expansion on the cofactor network presented by Varma et al. (*28*) and Varma and Palsson (*27*) is proposed. The additional reactions involving the cofactors are taken from Mathews and van Holde (*38*) and are summarized in Fig. 1. The inclusion of these reactions completes the picture of the cofactor network. The metabolic system is assumed to be at steady state. Therefore, the flux through each reaction must balance the rates of production and consumption of each metabolite in the system. For example, the flux balance around glucose-6-phosphate (*G6P*) would consist of the algebraic sum of incoming and outgoing fluxes:

$$J_1 + J_3 + J_{145} - J_2 - J_{15} - J_{144} = 0 \qquad (12)$$

J_i denotes the reaction fluxes associated with the production/consumption of *G6P*. Equation 12 constitutes an equality constraint. Since the system is at steady state, i.e., d[*G6P*]/dt = 0, the sum of the incoming fluxes will always equal the sum of the outgoing fluxes.

A limitation of the current model is that nitrogen assimilation has not been accounted for in the mathematical model. Similarly, oxygen uptake has only been accounted by way of the P/O ratio.

The above model has been formulated as a mathematical programming model and solved using GAMS (General Algebraic Modelling System).

Table 4
Optimum Production of Amino Acids

Amino acid	Theoretical yield $g \cdot g^{-1}$ sub. (A)	Literature values $g \cdot g^{-1}$ sub. (B)	Reference	% (B/A)
Alanine	0.989	—	—	—
Arginine	0.748	0.333	Yoshihara et al. (*46*)	44.1
Asparagine	1.144	—	—	—
Aspartate	1.342	—	—	—
Cysteine	0.655	—	—	—
Glutamate	0.817	0.555	Yoshihara et al. (*46*)	67.9
Glutamine	0.811	0.44	Yoshihara et al. (*46*)	54.3
Glycine	0.833	—	—	—
Histidine	0.643	0.12	Yoshihara et al. (*46*)	18.7
Isoleucine	0.534	0.261	Furukawa et al. (*47*)	48.9
Leucine	0.485	0.15	Yoshihara et al. (*46*)	30.9
Lysine	0.636	0.35	Yoshihara et al. (*46*)	—
Methionine	0.48	0.253	Dunyak et al. (*48*)	52.7
Phenylalanine	0.485	0.23	Park et al. (*39*)	47.4
Proline	0.633	—	—	—
Serine	1.167	0.708	Tanaka et al. (*49*)	60.7
Threonine	0.811	0.419	Furukawa et al. (*47*)	51.7
Tryptophan	0.469	0.4	Azuma et al. (*50*)	85.3
Tyrosine	0.511	0.09	Yoshihara et al. (*46*)	16.3
Valine	0.65	0.388	Tsuchida et al. (*43*)	59.7

RESULTS AND DISCUSSION

The model described in above has been used to study the biosynthesis of the 20 amino acids by *E. coli* with a view to identifying the limits to the stoichiometric capabilities of the metabolic network as well as the topological features of the relative pathway structures.

Quite predictably, the yield optimization of all 20 amino acids resulted in maximum yields at zero cell growth rate. The results are summarized in Table 4 which also includes literature values to provide a basis for comparison. The theoretical yields were obtained with glucose as the input substrate with a specific uptake rate of 10 $mmol \cdot g^{-1}$ $DW \cdot h^{-1}$. Although, this is very much a reference value and may well be unrealistic, it should not affect a yield optimization. These values, which have been determined in the absence of any maintenance energy requirements, represent the maximum theoretical stoichiometric production capability of the metabolic network. From a cursorary examination of Table 4, it emerges that while the experimental yields of some amino acids are close to the maximum attainable yields, this is not the situation obtained in the majority

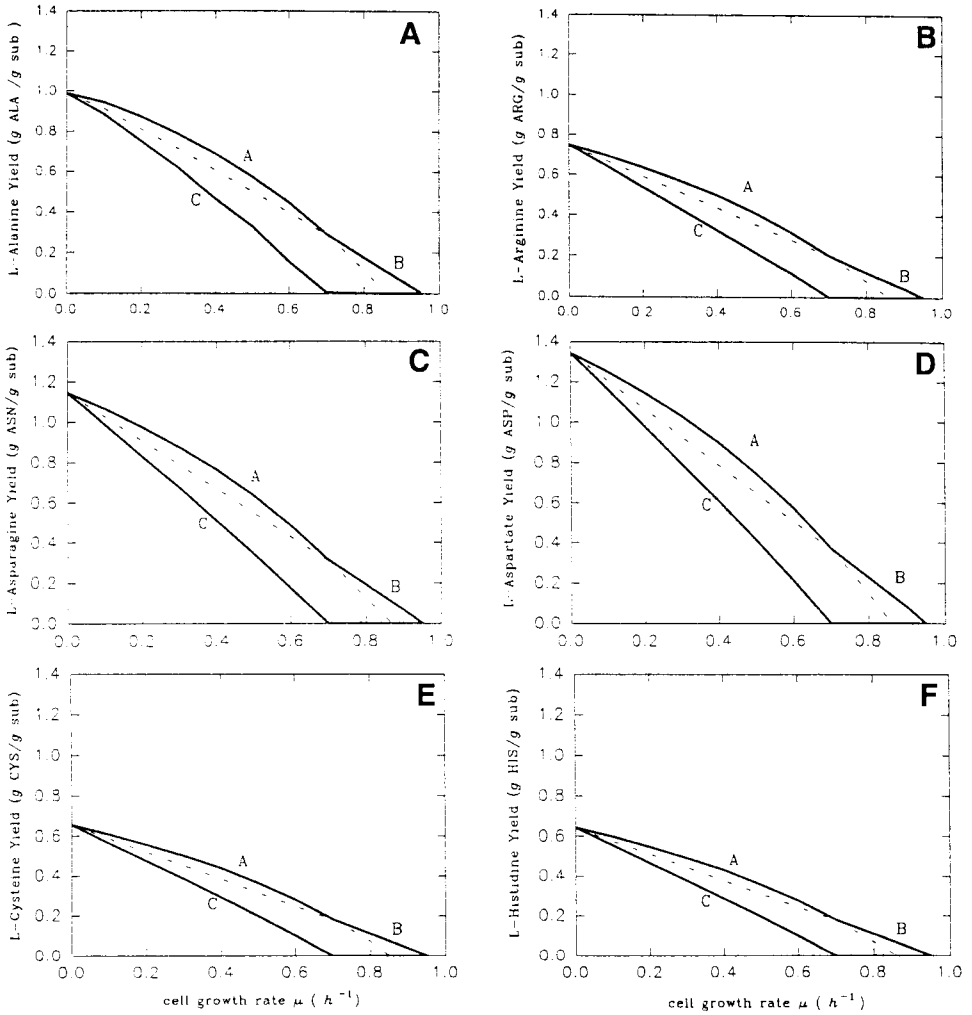

Fig. 2. Yields of amino acids: alanine (**A**), arginine (**B**), asparagine (**C**), asparatate (**D**), cysteine (**E**), and histidine (**F**), at various cell growth rates.

of cases. This, in turn, provides a lot of scope for further optimization studies. Having established the limits for cell growth rate and amino acid yield, the specific cell growth rate was varied in the range (0 – 0.9 h^{-1}) with a view to examine its effect on the flux of individual amino acids. Simulations were carried out for both constant and cell-growth-dependent *E. coli* composition at different cell growth rates and also at two levels of *ATP* demand; 45.13 and 117 mmol·g^{-1} DW. The yields obtained for the various amino acids at different cell growth rates are plotted in Fig. 2.

The area constrained by curves A, B, and C indicates the region of possible amino acid yields at different cell growth rates. As expected, the amount of amino acid produced decreases with increasing cell growth rate since under these conditions, more of the substrate has to be channelled toward biomass formation and less is available for amino acid pro-

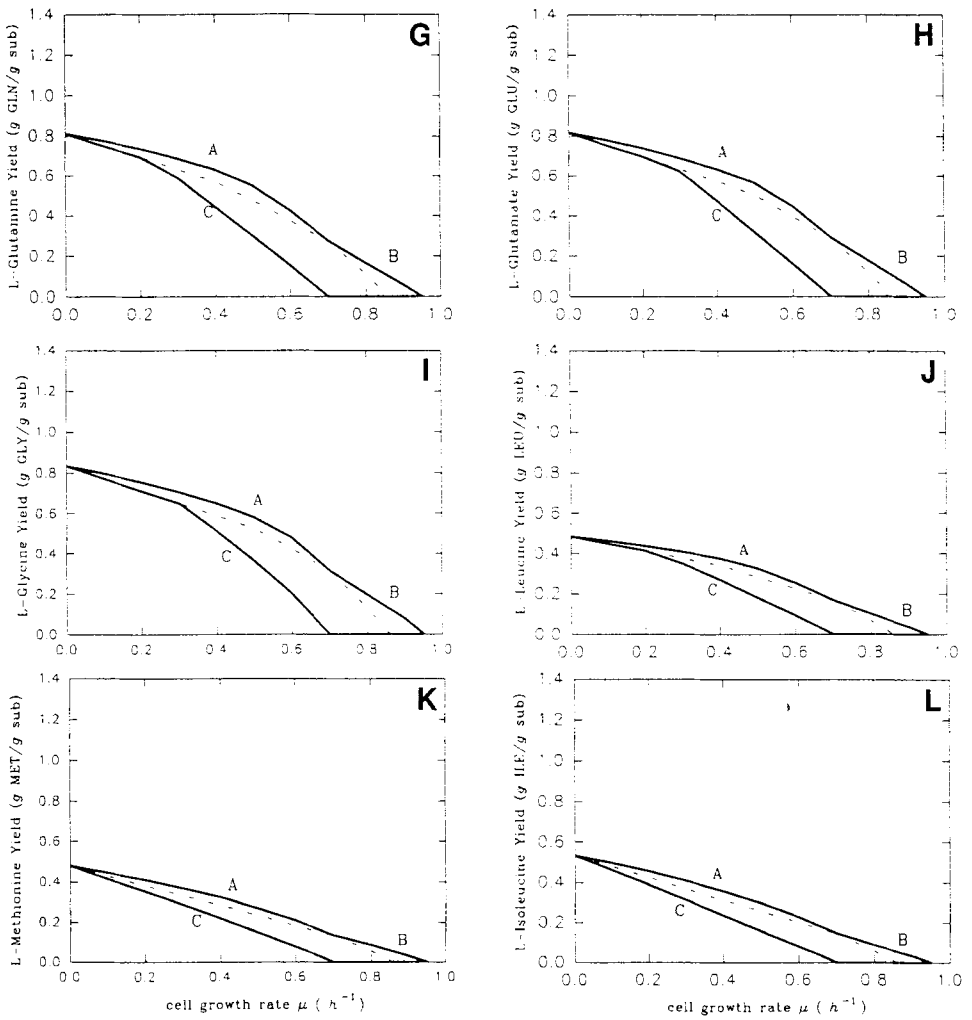

Fig. 2. (*cont'd*). Yields of amino acids: glutamine (**G**), glutamate (**H**), glycine (**I**), leucine (**J**), methionine (**K**), and isoleucine (**L**), at various cell growth rates.

duction. Curve A represents the maximum theoretical stoichiometric yields attainable with variable cell composition whereas curve B represents the maximum yields obtainable with fixed cell composition. The above curves refer to an *ATP* demand of 45.13 mmol·g^{-1} DW. Curve C on the other hand represents the growth yields attainable with fixed cell composition and an *ATP* demand of 117 mmol·g^{-1} DW. As expected, the decrease in amino acid yield is a linear function of the specific cell growth rate for constant cell composition (curves B and C) and a nonlinear function of the specific cell growth rate when the composition of the cells is assumed to depend on the cell growth rate. The higher *ATP* demand for biomass formation in curve C also means that a greater amount of substrate has to be oxidized to provide the energy needed for biomass formation, decreasing the amino acid yield.

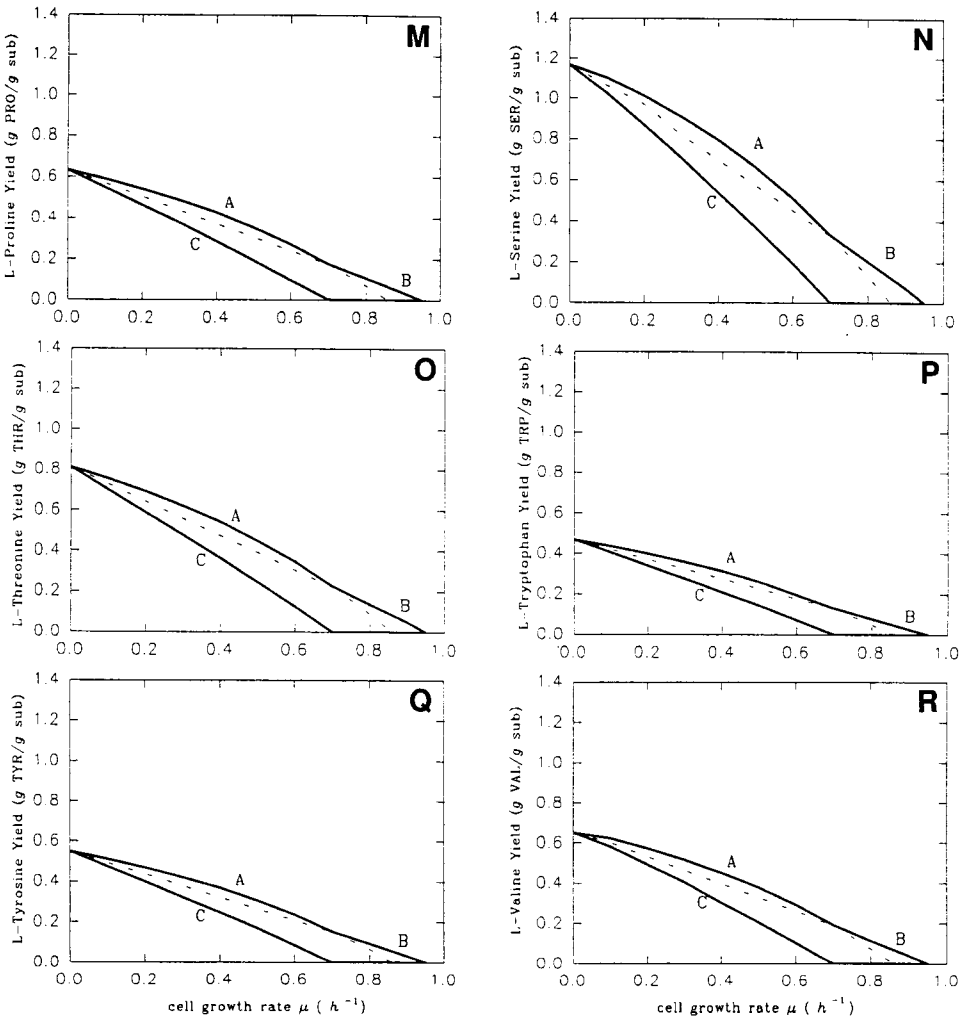

Fig. 2. (*cont'd*). Yields of amino acids: proline (**M**), serine (**N**), threonine (**O**), tryptophan (**P**), tyrosine (**Q**), and valine (**R**), at various cell growth rates.

An interesting observation relates to the behavior of curve A. At low specific cell growth rates, the yield obtained using the variable cell composition is in fact higher than that obtained using the constant cell composition assumption. The opposite is true at higher cell growth rates. This can be explained by the fact that, at low cell growth rates a lesser amount of amino acid is required for biomass formation in the variable cell composition model. The smaller amount of amino acids being channelled to biomass formation for curve A has thus resulted in a higher amino acid yield. The opposite argument holds at high cell growth rates.

It is evident from Fig. 2 that different amino acids have different yields. The highest yields obtained for growth on glucose were for alanine (*Ala*), asparagine (*Asn*), aspartate (*Asp*), and serine (*Ser*). These results can be easily verified at zero cell growth rate by writing down the appropriate stoichiometric balances. Two examples are given below:

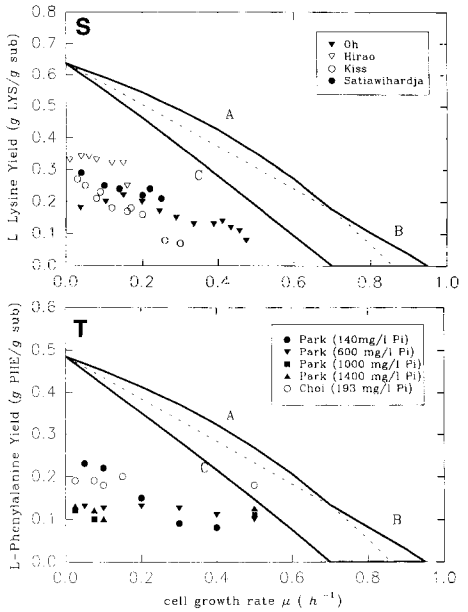

Fig. 2. (*cont'd*). Theoretical and experimental yields of amino acids lysine (**S**) and phenylalanine (**T**), at various cell growth rates. For data sources in S, *see* refs. *11a*, *21a*, and *24*.

Stoichiometric Balance for Serine (*Ser*)

$$C_6H_{12}O_6 + O_2 + 2NH_3 \rightarrow 2C_3H_7O_3N + 2H_2O$$

Yield of *Ser* = 2 × 105/180 = 1.167 g/g glucose.

Stoichiometric Balance for Phenylalanine (*Phe*)

$$2C_6H_{12}O_6 + 2O_2 + NH_3 \rightarrow C_9H_{11}O_2N + 8H_2O + 3CO_2$$

Yield of *Phe* = 165/(2 × 180) = 0.458 g/g glucose.

It can be easily seen from these balances that *Ser* is produced more efficiently, i.e., at much higher yields, than *Phe* as there is no loss of carbon in the form of carbon dioxide. Loss of carbon as carbon dioxide can be attributed to the need for *ATP*, *NADPH*, and *NADH* in the formation of the amino acid. The production of *Ser* does not require any *NADPH* or *NADH*:

$$3PG + Glu \rightarrow Ser + \alpha KG + NADH + Pi \qquad \text{(Reac. No. 85)}$$

On the other hand, production of *Phe* requires *NADPH*.

$$2PEP + E4P + ATP + \mathbf{NADPH} \rightarrow Chor + ADP + 4\,Pi \qquad \text{(Reac. No. 64)}$$

$$Chor + Glu \rightarrow Phe + \alpha KG + CO_2 \qquad \text{(Reac. No. 65)}$$

NADPH is mainly supplied via the reaction: *G6P* → *R5P* + CO_2 + ***2NADPH*** (Reac. No. 15) in the pentose phosphate shunt. As can be seen, there is loss of carbon in the form of carbon dioxide. Hence, it may be concluded

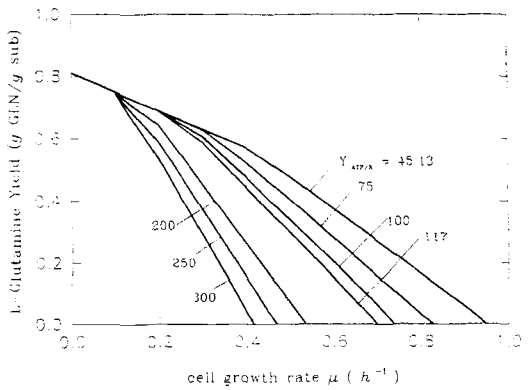

Fig. 3. Glutamine yields as a function of $Y_{ATP/X}$.

that the more carbon is being lost as carbon dioxide in the reactions involved in the production of the desired amino acid, the lower the amino acid yield will be.

All but four amino acids (glutamine [*Gln*], glutamate [*Glu*], glycine [*Gly*], and leucine [*Leu*]) show similar trends in their relationship between cell growth and amino acid yield. From Fig. 2G, it can be seen that at low cell growth rates ($\mu < 0.2\ h^{-1}$) and for fixed cell composition, the yields for *Gln* do not depend on *ATP* demand, i.e., the solid line of curve C coincides with the dotted part of curve B. In addition, the amino acid yield does not decrease linearly with growth rate which would be the case for fixed cell composition. This has resulted in some sort of 'switching point' where the graph has two different gradients. The same phenomenon can be observed for *Glu, Gly,* and *Leu* (Fig. 2H, I, J). This unique behavior deviates from the norm where amino acid yields decrease with increasing *ATP* demand. A more detailed examination of the yield of *Gln* with cell growth rate was carried out with $Y_{ATP/X}$ as the parameter. The result of this investigation is shown in Fig. 3.

As $Y_{ATP/X}$ increases, the *Gln* yield decreases and the 'switching points' in the graphs occur at lower cell growth rates. Worth noting is that the metabolic system becomes less sensitive to the increase in $Y_{ATP/X}$ at high values of $Y_{ATP/X}$ as indicated by the smaller changes in the slopes of the graphs. A possible explanation for this behavior may be that at low cell growth rates, more *ATP* is generated than is actually needed for biomass formation. The production capability is thus limited by the metabolic system and not by energy requirements. As the demand for *ATP* increases, the amino acid yield decreases as the system is now limited by energy requirements.

In order to investigate how far these theoretical yields are from experimental ones, experimental yields for *Lys* and *Phe* collected from the literature have been included in Fig. 2S and T. From these two figures, it can be easily deduced that although the experimental results follow a similar

Table 5
Amounts of Various Amino Acids
Produced by 2-thiazolealanine Resistant
Mutant of *Brevibacterium* (*43*)

Amino acid	Yield (mg/l)
Valine	31.0
Glutamic acid	2.1
Alanine	1.5
Lysine	4.0
Leucine	1.0
Isoleucine	1.0

trend, they are way below the values predicted by the model. It has to be mentioned that although the organism used for *Phe* production (*39,40*) is *E. coli*, the organisms producing *Lys* are not *E. coli* but *C. glutamicum* and *B. lactofermentum*. Hence, it is not possible to obtain a direct comparison between theoretical and experimental yields for *Lys* production. In addition, no experimental yields could be obtained for cell growth rates higher than 0.5 h^{-1} or indeed at zero cell growth rate.

There are several possible reasons for the observed disparity between theoretical and experimental yields. First of all, it should be considered that this model is based entirely on stoichiometric information with no information on metabolic regulation and feedback inhibition which will certainly place additional constraints on the network (*1*). Since this computer model does not take into account reaction kinetic constraints, it is bound to produce higher amino acid yields.

A second reason could be the existence of energy dissipation reactions. Possible energy dissipation mechanisms include accumulation of polymeric products, dissipation of heat by "ATPase mechanisms" and activation of shunt mechanisms that either bypass energy-yielding reactions or require a greater amount of energy for priming. One futile cycle that may be used for energy dissipation in *E. coli* is the interconversion of fructose-6-phosphate and fructose-1,6-phosphate (*41,42*). Activation of such cycles would result in lower experimental yields and hence account for the discrepancy between theoretical and experimental yields.

Finally, the production of by-products should not be underestimated. Tuschida et al. (*43*) observed that besides the production of valine (*Val*) which was the desired product, other amino acids were also being produced in quantities greater than that required by biosynthesis (Table 5). This diversion of glucose to the production of other amino acids in quantities greater than those required for biosynthesis has reduced the overall yield of *Val*. Although the objective of this model has been to identify the maximum possible yields in the absence of byproducts, it may well be that, in certain cases, this is not a practical proposition.

Table 6
States of the Metabolic System for Lysine Production and their Characteristics

Specific cell growth rate range (h^{-1})	Characteristics
0	Glyoxylate shunt inactive, only central pathways active
0.01–0.24	Glyoxylate shunt inactive, pathways to cell constituents active
0.25–0.62	Glyoxylate shunt active, pathways to cell constituents active
0.63–0.70	Reaction: $Pyr + 2ATP \rightarrow PEP + 2ADP + Pi$ vanishes, Reaction: $\alpha KG \rightarrow SuccCoA + NADH + CO_2$ activates
0.71–0.77	Reaction: $F6P \rightleftharpoons G6P$ changes direction
0.78–0.90	Reaction: $Succ + GTP \rightleftharpoons SuccCoA + Pi + GDP$ changes direction

FLUX MAPS

In order to understand the regulation of amino acid production, graphical representations of the net fluxes in the metabolic network were produced for a number of cell growth rates. The amino acid *Lys* has been chosen as a first model system since a lot of research appears to have gone into understanding its biological production.

Only the net fluxes through the central pathways (glycolysis, gluconeogenesis, pentose phosphate shunt, TCA cycle) and the pathways leading to the amino acid formation are shown in the simplified flux distribution maps. The reason for not including some of the nonzero net fluxes is their relatively low contribution towards the regulation of *Lys* production; all the metabolites which have been left out are involved in biomass formation and their fluxes are directly proportional to the cell growth rate, making them fairly predictable. As a result, one may find that the fluxes on the figures do not always balance. A comparison of cell growth rates for the production of *Lys* reveals some interesting topological differences in the flux distribution maps obtained at different cell growth rates. A closer examination of the 0 to 0.9 h^{-1} range was carried out to trace the cell growth rates at which these changes occur. These cell growth rates, henceforth will be treated as *"switch points"* indicating a transition from one metabolic state to another. Table 6 and Figure 4 summarize these metabolic states. It should be considered that the actual values of the fluxes at different cell growth rates are not of great significance because of the assumption of an arbitrary specific substrate uptake rate of 10 $mmol.g^{-1}\,DW.h^{-1}$. However, what is important is the sequence of metabolic events which should take place with increasing cell growth rate in order to guarantee overproduction of *Lys* by the metabolic system.

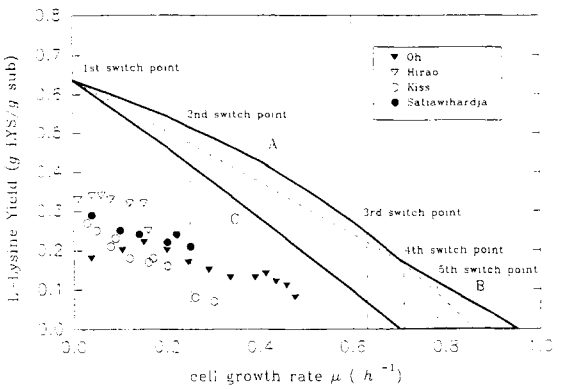

Fig. 4. Calculated and experimental lysine yields. The states of the metabolic systems and the relevant switch points are highlighted.

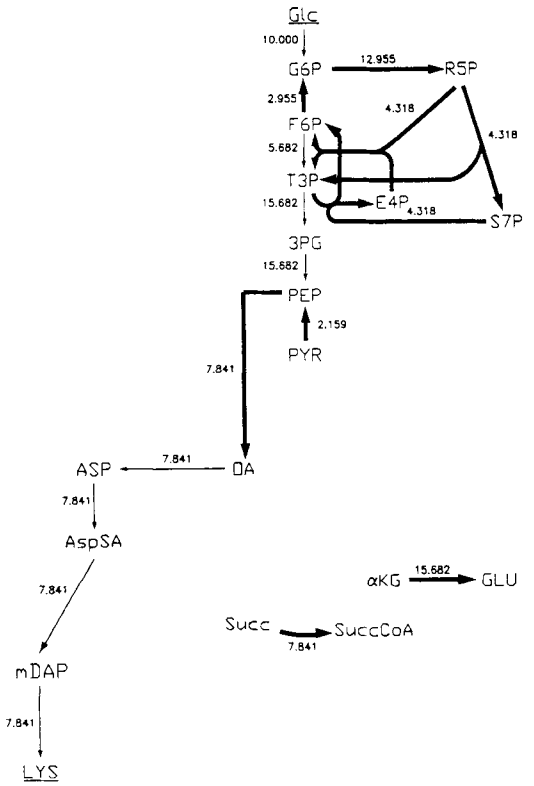

Fig. 5. A simplified map of the net fluxes throughout the reaction network, for maximum lysine production at $\mu = 0\ h^{-1}$.

$\mu = 0\ h^{-1}$

As expected, at zero cell growth rate there is no need for metabolites to be involved in biomass formation and, consequently, all the nonrelevant pathways have been shut down (Fig. 5). It is worth noting that at

zero cell growth rate, the TCA cycle is not activated indicating that there is no need for large amounts of *NADH* and *ATP*. Indeed, the amount of *ATP* and *NADH* produced by reaction No. 6 appears to suffice for the metabolic system at zero cell growth rate, making the activation of the TCA cycle unnecessary.

$$T3P + ADP + Pi \rightarrow 3PG + \mathbf{ATP} + \mathbf{NADH} \qquad \text{(Reac. No. 6)}$$

Phosphoenolpyruvate (*PEP*) appears to be converted directly to oxaloacetate (*OA*) by the following reaction which is part of the carboxylation cycle:

$$PEP + CO_2 \rightarrow OA + P_i \qquad \text{(Reac. No. 26)}$$

This is clearly a more efficient means of producing *Lys* than through the TCA cycle as there is no loss of carbon in the form of carbon dioxide.

Another interesting observation is that the reaction linking fructose-6-phosphate (*F6P*) to *G6P* is directed towards *G6P* formation: *F6P* → *G6P* (Reac. No. 3). This is rather peculiar and it is opposite to the rest of the glycolytic steps. The reversed in flux from *F6P* to *G6P* is due to the relatively large flux from *G6P* to ribulose-5-phosphate (*R5P*): *G6P* → *R5P* + CO_2 + *NADPH* (Reac. No. 15) which, in turn, indicates a large demand for *NADPH*. This has resulted in the activation of the pentose phosphate shunt (*PPS*) even though there is no biomass formation at zero cell growth rate. The high demand for *NADPH* is due to the fact that formation of every mole of *Lys* requires two moles of *NADPH*.

$$Asp + ATP + \mathbf{NADPH} \rightarrow ASPSA + ADP + Pi \qquad \text{(Reac. No. 71)}$$

$$ASPSA + Pyr + Glu + SuccCoA + \mathbf{NADPH} \rightarrow mDAP + Succ + aKG \qquad \text{(Reac. No. 72)}$$

$$mDAP \rightarrow Lys + CO_2 \qquad \text{(Reac. No. 73)}$$

The second reaction step which is opposite to the rest of the glycolytic steps is the reaction linking phosphoenolpyruvate (*PEP*) to pyruvate (*Pyr*). This is directed towards *PEP* formation: *Pyr* + 2ATP → *PEP* + 2*ADP* + *Pi* (Reac. No. 11), which indicates that there is relatively a large need for *PEP* in the system. The total flux to *PEP* amounts to 17.841 mmol·g^{-1} DW·h^{-1}. Indeed, *PEP* is needed as a carrier molecule for importing glucose into the cell (reaction No. 1: *Glc* + *PEP* → *Pyr* + *G6P*). This reaction accounts for 10 mmol·g^{-1} DW·h^{-1} of *PEP* consumed which is not shown in Fig. 5. The remaining 7.841 mmol·g^{-1} DW·h^{-1} is directed towards *OA* production (Reaction No. 26).

$$Glc + PEP \rightarrow Pyr + G6P \qquad \text{(Reac. No. 1)}$$

10 mmol·g^{-1} DW·h^{-1} of *Pyr* is formed from Reaction No. 1, of which 2.159 mmol·g^{-1} DW·h^{-1} is directed towards *PEP* formation, the remaining 7.841 mmol·g^{-1} DW·h^{-1} being consumed in Reaction No. 72.

Another point worth noting is the two isolated reactions from succinate (*Succ*) to succinyl-CoA (*SuccCoA*) and from α-ketoglutarate (*αKG*) to

Glu in the TCA cycle. The net flux from *Succ* to *SuccCoA* has exactly the same value as the flux leading to *Lys* formation. This is because both compounds are involved in *Lys* synthesis.

The formation of one mole of *Lys* requires two moles of *Glu* which accounts for the fact that the value of the flux from αKG to *Glu* is twice that of the flux leading to *Lys* production. The reason for large amounts of *Glu* being formed at zero cell growth rate is that *Glu* provides the necessary amino group for *Lys* formation. Although *αKG* appears to be synthesized from nothing in Fig. 5, it is actually a byproduct of the following reactions.

$$OA + \mathbf{Glu} \rightarrow Asp + \alpha KG \qquad \text{(Reac. No. 69)}$$

$$ASPSA + Pyr + \mathbf{Glu} + SuccCoA + NADPH \rightarrow mDAP + Succ + \alpha KG \qquad \text{(Reac. No. 72)}$$

$$mDAP \rightarrow Lys + CO_2 \qquad \text{(Reac. No. 73)}$$

$\mu = 0.1\ h^{-1}$

At this cell growth rate, the pathways leading to amino acids and nucleotide synthesis, as well as those leading to the production of biomass constituents are now been activated (Fig. 6). The net fluxes through these pathways have been adjusted to meet the metabolic demands dictated by the cell growth rate, in addition to those leading to *Lys* production.

An interesting observation is the increased flux through the *PPS*. The flux linking *G6P* to *R5P*: *G6P* → *R5P* + CO_2 + 2 *NADPH* (Reac. No. 15) has now increased by 2.8%. The increased flux may be attributed to the dependence of biosynthesis on redox energy. The demand for *NADPH* increases with cell growth rate and, as the *PPS* is the major producer of *NADPH*, it seems appropriate that the flux towards this pathway should be increased.

Another important feature is the activation of a reaction which converts acetate (*Ac*) to acetyl-CoA (*AcCoA*): *Ac* + *ATP* → *AcCoA* + *ADP* + *Pi* (Reac. No. 33). *Ac* is a byproduct of several reactions which produce biosynthetic precursors:

$$2Glu + AcCoA + ATP + NADPH \rightarrow Orn + \mathbf{Ac} + \alpha KG + ADP + Pi \qquad \text{(Reac. No. 82)}$$

$$Ser + AcCoA + H_2S \rightarrow Cys + \mathbf{Ac} \qquad \text{(Reac. No. 87)}$$

$$3ADPHep + 2ADPGlc + 3CDPEtN + 3CMPKDO + 2UDPNAG + 2C14{:}0 + 4C14{:}1 + ATP \rightarrow LPS + 3CDP + 3CMP + UDP + 2\mathbf{Ac} + 6ADP + PPi + 2Pi \qquad \text{(Reac. No. 137)}$$

Ac re-enters the metabolic network and is directed towards the TCA cycle—which is the major producer of biosynthetic precursors—via acetyl-CoA.

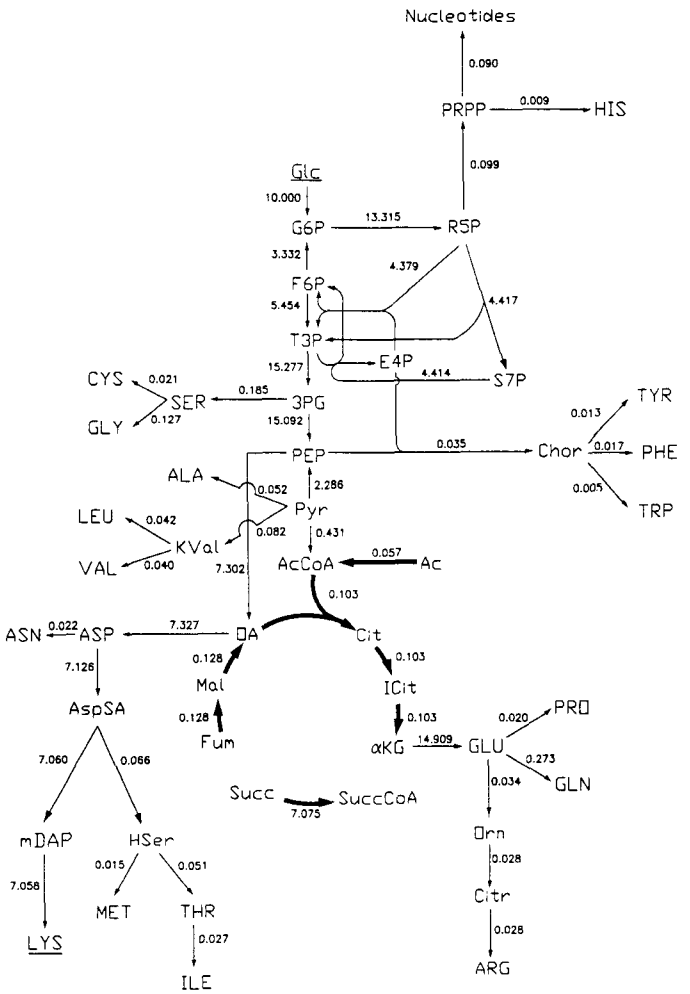

Fig. 6. A simplified map of the net fluxes throughout the reaction network, for maximum lysine production at $\mu = 0.1\ h^{-1}$.

The TCA cycle is now partly activated. Fumarate (*Fum*), like acetate is a by-product of various biosynthetic reactions:

$$\text{Citr} + \text{Asp} + \text{ATP} \rightarrow \text{Arg} + \mathbf{\text{Fum}} + \text{AMP} + \text{PPi} \qquad \text{(Reac. No. 84)}$$

$$\text{PRPP} + 2\text{Gln} + \text{Gly} + \text{Asp} + 4\text{ATP} + \text{CO}_2 \rightarrow \text{PRAIC} + 2\text{Glu} + \mathbf{\text{Fum}} + \text{Asp} + 4\text{Pi} + \text{PPi} + \text{THF} \qquad \text{(Reac. No. 94)}$$

$$\text{IMP} + \text{Asp} + \text{GTP} \rightarrow \text{AMP} + \mathbf{\text{Fum}} + \text{GDP} + \text{Pi} \qquad \text{(Reac. No. 96)}$$

Fum enters the TCA cycle so as to generate *NADH* on conversion to *OA*. The *NADH* produced in Reaction No. 47 then undergoes oxidative phosphorylation in the electron transport system to generate *ATP* for biomass formation.

$$\text{Fum} \rightarrow \text{Mal} \qquad \text{(Reac. No. 45)}$$

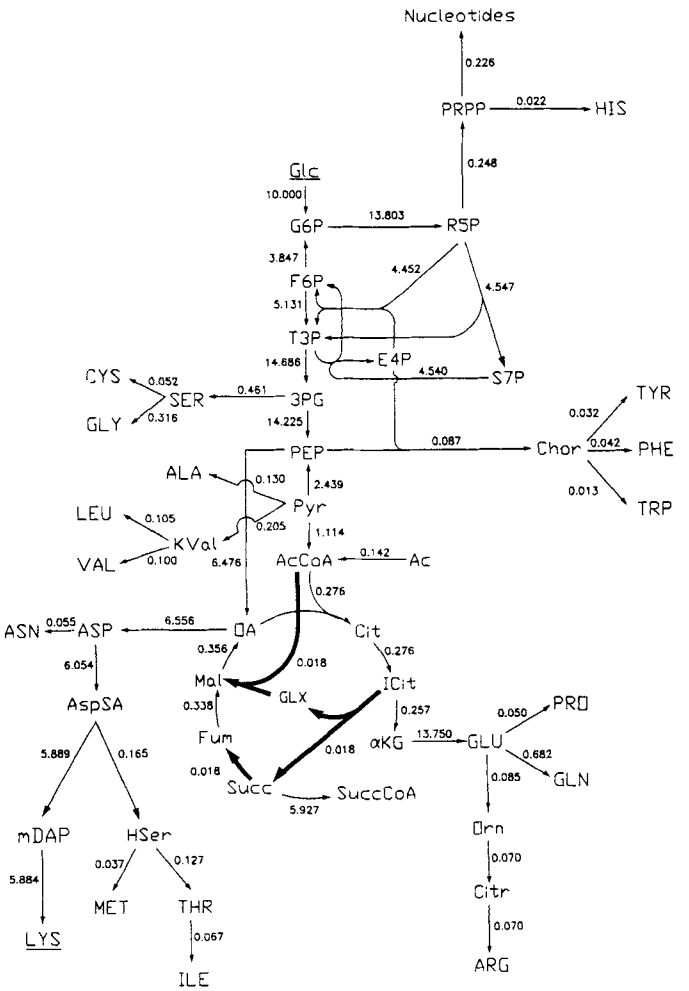

Fig. 7. A simplified map of the net fluxes throughout the reaction network, for maximum lysine production at $\mu = 0.25\ h^{-1}$.

$$Mal \rightarrow OA + \mathbf{NADH} \qquad \text{(Reac. No. 47)}$$

It has also been found that the value of the flux from *Succ* to *SuccCoA* has decreased from 7.841 mmol·g^{-1} DW·h^{-1} at $\mu = 0\ h^{-1}$ to 7.075 mmol·g^{-1} DW·h^{-1} at $\mu = 0.01\ h^{-1}$. The value of the flux involving *Succ* and *SuccCoA* is very much affected by the production of *Lys* since this is a significant flux in the metabolic system at low cell growth rates.

$\mu = 0.25\ h^{-1}$

At a cell growth rate of 0.25 h^{-1}, the glyoxylate shunt is activated (Fig. 7). As the cell growth rate increases, the biosynthetic load on the network also increases. The biosynthetic pathways which produce the metabolites involved in biomass formation are now switched on and the central pathways which provide such precursors, one of which is *OA*,

have to cope with the increased demand. Such compounds need to be replenished as the TCA cycle activity would otherwise cease.

Replenishment of *OA* up to $\mu = 0.24\ h^{-1}$ is solely by the reaction: *PEP* + CO_2 → *OA* + P_i (Reac. No. 26) which is part of the carboxylation cycle. At $\mu = 0.25\ h^{-1}$, the glyoxylate shunt becomes active and takes over some of the load for *OA* replenishment. A glyoxylate shunt simply provides a convenient shortcut with the net synthesis of one additional compound in the TCA cycle, i.e., isocitrate (*ICit*) which is converted to *Succ* and glyoxylate (*GLX*). *GLX* may be converted to malate on reaction with *AcCoA*.

$$\text{ICit} \rightarrow \text{GLX} + \text{Succ} \qquad \text{(Reac. No. 48)}$$

$$\text{GLX} + \text{AcCoA} \rightarrow \text{Mal} \qquad \text{(Reac. No. 49)}$$

Associated with the activation of the glyoxylate shunt is the activation of the reaction: *Succ* → *Fum* + *FADH* (Reac. No. 44) which has the same flux as that of the glyoxylate shunt. Besides replenishing the *OA* drawn for amino acid formation, there is an additional reason for the activation of the glyoxylate shunt. As the cell growth rate increases, the reaction fluxes in the TCA cycle have to increase in order to cope with the increased *ATP* demand. As less material is available for *OA* synthesis via the reaction: *PEP* + CO_2 → *OA* + P_i, the glyoxylate shunt, which is an alternative route for the replenishment of *OA*, is activated. In addition, *Mal* and *Succ* on conversion to *OA* produce redox energy in the form of *NADH* and *FADH*.

$$\text{SUCC} \rightarrow \text{Fum} + \mathbf{FADH} \qquad \text{(Reac. No. 44)}$$

$$\text{Fum} \rightarrow \text{Mal} \qquad \text{(Reac. No. 45)}$$

$$\text{Mal} \rightarrow \text{OA} + \mathbf{NADH} \qquad \text{(Reac. No. 47)}$$

The redox energy produced in the TCA cycle can be converted to *ATP* in the electron transport system. This additional source of *ATP* is used to cope with the increased demand for *ATP* due to additional biomass formation as the cell growth increases.

$\mu = 0.63\ h^{-1}$

One prominent feature of the flux map at $\mu = 0.63\ h^{-1}$ is that the reaction: *Pyr* + *2ATP* → *PEP* + *2ADP* + *Pi* (Reac. No. 11) has now completely disappeared (Fig. 10). The fluxes leading to the amino acids of the alanine family, which are essential for biomass formation,

$$\text{Pyr} + \text{Glu} \rightarrow \alpha\text{KG} + \text{Ala} \qquad \text{(Reac. No. 88)}$$

$$2\text{Pyr} + \text{NADPH} \rightarrow \text{Kval} + CO_2 \qquad \text{(Reac. No. 89)}$$

consume a significant amount of *Pyr*. The metabolic system can no longer afford the reaction degrading *Pyr* to *PEP*. Therefore, this reaction has to be shut down.

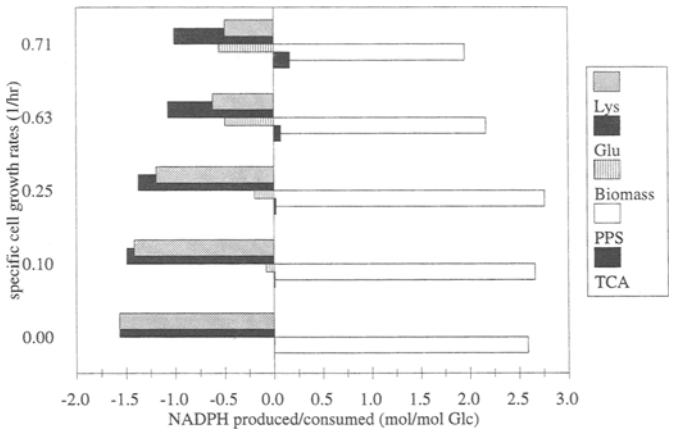

Fig. 8. *NADPH* requirement during the production of L-lysine.

It is also observed that, at this growth rate, there is a decrease in *NADPH* production by the *PPS*. Production of *Lys* is unique in its high demand for reducing power as shown below:

$$\text{OA} + \text{Glu} \rightarrow \text{Asp} + \alpha\text{KG} \qquad \text{(Reac. No. 69)}$$

$$\text{Asp} + \text{ATP} + \textbf{NADPH} \rightarrow \text{ASPSA} + \text{ADP} + \text{Pi} \qquad \text{(Reac. No. 71)}$$

$$\text{ASPSA} + \text{Pyr} + \text{Glu} + \text{SuccCoA} + \textbf{NADPH} \rightarrow \text{mDAP} + \text{Succ} + \alpha\text{KG} \qquad \text{(Reac. No. 72)}$$

$$\text{mDAP} \rightarrow \text{Lys} + \text{CO}_2 \qquad \text{(Reac. No. 73)}$$

The production and consumption of *NADPH* at various growth rates are plotted in Fig. 8. The TCA cycle and the pentose phosphate shunt are the major producers of *NADPH* whereas the production of *Glu*, *Lys*, and biomass make up the major consumers of *NADPH*.

In most cellular growth processes, an increase in the production of *NADPH* is often observed at higher cell growth rates due to the increase in the amount of *NADPH* needed for biomass formation.

With *Lys* production, the overall comsumption of *NADPH* does not necessarily increase with cell growth rate even though there is a steady increase in the consumption of *NADPH* for biomass formation. This increase, however, is balanced by the concurrent decrease in *NADPH* consumption for the production of *Lys*, the yield of which decreases with increasing cell growth rate. Production of *NADPH* by the *PPS* increases from 25.910 $\text{mmol}\cdot\text{g}^{-1}\,\text{DW}\cdot\text{h}^{-1}$ at $\mu = 0\ \text{h}^{-1}$ to 27.606 $\text{mmol}\cdot\text{g}^{-1}\,\text{DW}\cdot\text{h}^{-1}$ at $\mu = 0.25\ \text{h}^{-1}$ after which it decreases. The initial increase in *NADPH* production may be attributed to the demand for biomass formation as the cell growth rate increases. However, at high cell growth rates, the decrease in *NADPH* consumption due to lesser amounts of *Lys* produced is greater than the increase demand for *NADPH* due to biomass formation, resulting in smaller total amounts of *NADPH* being produced.

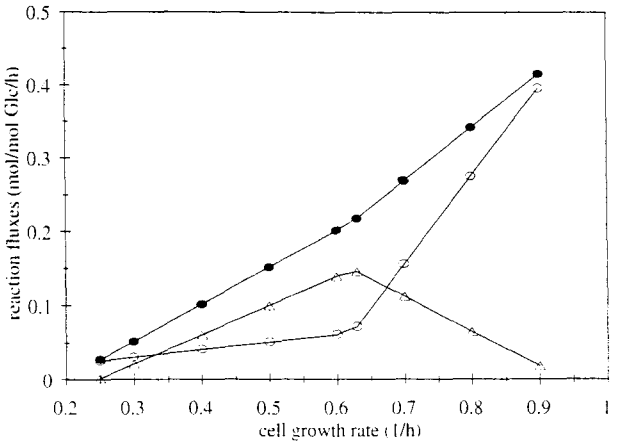

Fig. 9. Effect of specific cell growth rate on metabolic fluxes: (△) glyoxylate shunt, reaction: (○) *Cit* → *ICit* and reaction: (●) *ICit* → *αKG* + CO_2 + *NADPH*.

Another interesting point is the activation of the reaction: *αKG* → *SuccCoA* + *NADH* + CO_2 (Reac. No. 41), resulting in a fully-functional TCA cycle. The full activation of the TCA cycle is due to the increased *ATP* demand at high cell growth rates. At the same time, the flux through the glyoxylate shunt increases from 0.018 mmol·g^{-1} DW·h^{-1} at μ = 0.25 h^{-1} to a peak value of 1.459 mmol·g^{-1} DW·h^{-1} at μ = 0.63 h^{-1} and then it decreases again (Fig. 9). A closer examination of the reactions resulting in the formation and consumption of *ICit*, the starting compound of the glyoxylate shunt:

$$\text{Cit} \rightarrow \text{ICit} \qquad \text{(Reac. No. 37)}$$

$$\text{ICit} \rightarrow \alpha\text{KG} + \text{CO}_2 + \text{NADPH} \qquad \text{(Reac. No. 39)}$$

shows that the flux values through the above reactions increase with cell growth rate. Furthermore, a kink is observed in the graphs at μ = 0.63 h^{-1} which corresponds to the peak in flux through the glyoxylate shunt. It is also worth observing that when μ > 0.63 h^{-1}, the flux through the reaction: ICit → *αKG* + CO_2 + *NADPH* increases at a faster rate than when μ < 0.63 h^{-1}. This is to compensate for the decrease in flux through the glyoxylate shunt. The unique trend in the flux through the glyoxylate shunt highlights its role in the replenishment of *OA* drawn off for amino acid production. As mentioned above, the activation of the glyoxylate shunt is to alleviate the load on the carboxylation cycle for the replenishment of *OA* and to produce *NADH* and *FADH* as cell growth rate increases. However, at high cell growth rates, the demand for *OA* decreases due to the smaller amounts of *Lys* being produced and reduces the load on the glyoxylate shunt. Thus, a maximum in the flux through the glyoxylate shunt is observed.

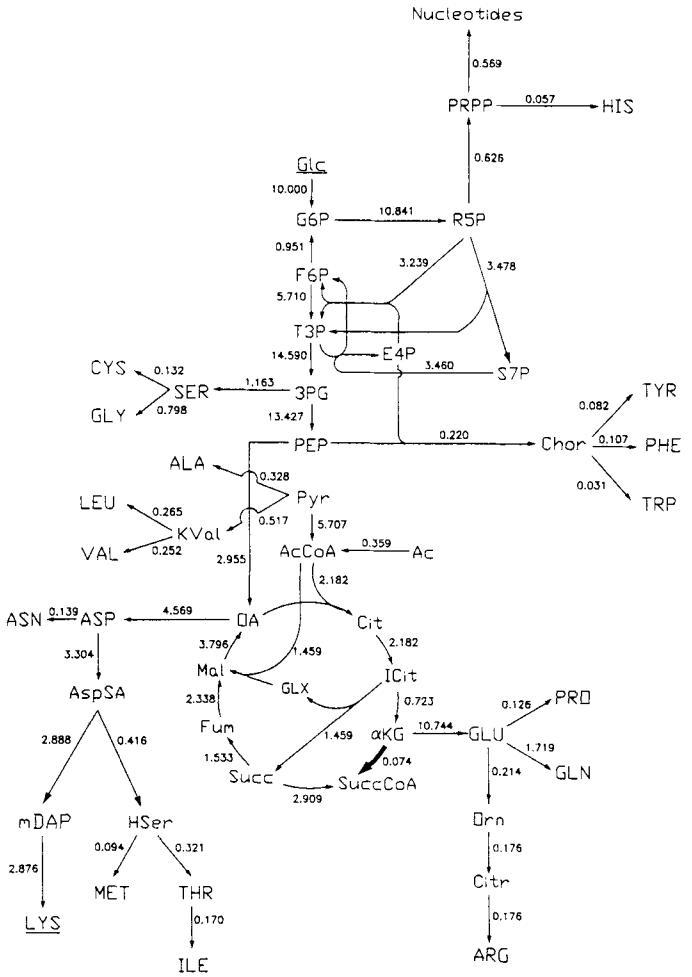

Fig. 10. A simplified map of the net fluxes throughout the reaction network, for maximum lysine production at $\mu = 0.63\ h^{-1}$.

$\mu = 0.71\ h^{-1}$

Up to a cell growth rate of 0.70 h^{-1}, the reaction connecting *F6P* and *G6P* is directed towards *G6P* formation. The flux of the backward reaction: *F6P* → *G6P* (Reac. No. 3) decreases as the cell growth rate increases until, at $\mu = 0.71\ h^{-1}$, the forward reaction: *G6P* → *F6P* (Reac. No. 2) is activated (Fig. 11). The reason for the reversal in the direction of the reaction: *F6P* ⇌ *G6P* is the apparent decrease in the flux of *PPS* reaction: G6P → *R5P* + CO_2 + *2NADPH* (Reac. No. 15). As the amount of *NADPH* required for *Lys* production decreases with increasing cell growth rate, less *G6P* has to be channelled to the *PPS*.

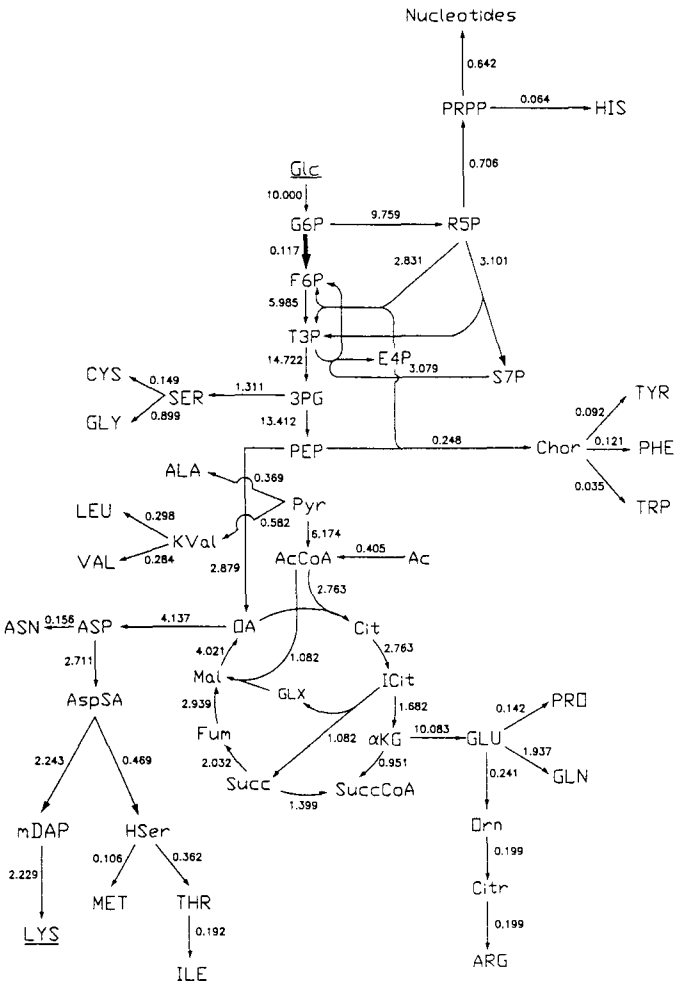

Fig. 11. A simplified map of the net fluxes throughout the reaction network, for maximum lysine production at $\mu = 0.71\ h^{-1}$.

μ = 0.79 h^{-1}

Of particular interest at this growth rate is the shift in the direction of the reaction converting succinate *Succ* to *SuccCoA* in the TCA cycle (Fig. 12). The flux of the backward reaction: *Succ* + *GTP* → *SuccCoA* + *Pi* + *GDP* (Reac. No. 43) decreases as the cell growth rate increases until, at $\mu = 0.79\ h^{-1}$, the forward reaction: *SuccCoA* + *Pi* + *GDP* → *Succ* + *GTP* (Reac. No. 42) is activated. *Succ* and *SuccCoA* are involved in the production of Lys and methionine (*Met*).

$$\text{ASPSA} + \text{Pyr} + \text{Glu} + \mathbf{\text{SuccCoA}} + \text{NADPH} \rightarrow \text{mDAP} + \mathbf{\text{Succ}} + \alpha\text{KG} \qquad \text{(Reac. No. 72)}$$

$$\text{mDAP} \rightarrow \text{Lys} + CO_2 \qquad \text{(Reac. No. 73)}$$

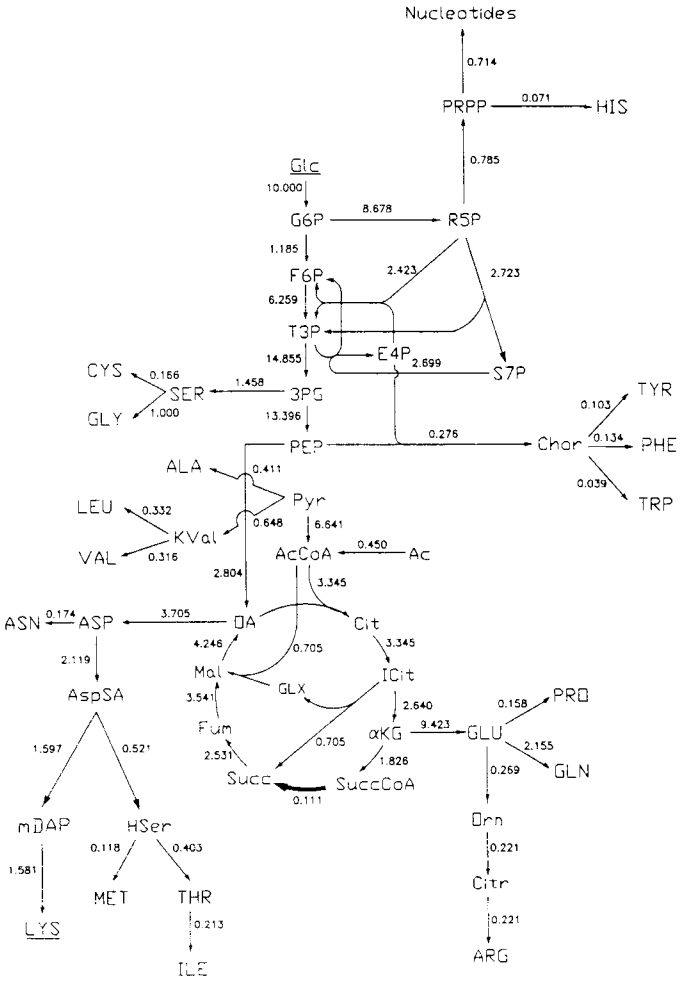

Fig. 12. A simplified map of the net fluxes throughout the reaction network, for maximum lysine production at $\mu = 0.79\ h^{-1}$.

$$\text{HSer} + \text{Cys} + \textbf{SuccCoA} + \text{MTHF} \rightarrow \text{Met} + \text{Pyr} + \textbf{Succ} + NH_3 + \text{THF} \qquad \text{(Reac. No. 75)}$$

At low cell growth rates, the *SuccCoA* needed for *Lys* and *Met* is produced from *Succ* via Reaction No. 43. As the cell growth rate increases, the amount of *Succ* produced from Reaction No. 72 decreases due to the lower amounts of *Lys* being produced. At the same time, the fluxes of the reactions in the TCA cycle have now increased so that, at $\mu = 0.79\ h^{-1}$, the *SuccCoA* production rate via the reaction: *αKG → SuccCoA + NADH + CO_2* (Reac. No. 41) is greater than its comsumption rate for *Lys* and *Met* production (1.826 vs 1.715 mmol·g^{-1} DW·h^{-1}). Hence, the forward reaction that converts *SuccCoA* to *Succ* is activated.

Table 7
Gibbs-energy Dissipation for Heterotrophic Growth
and Degree of Reduction of Various Substrates

Substrate	No. of C-atoms	γ_s	$(D_s/r_x)_{gr}$ kJ/C-mol
Citrate	6	3.00	550
Glucose	6	4.00	200
Glycerol	3	4.66	400
Lactate	3	4.00	400

OTHER SUBSTRATES

Besides glucose, a number of other carbon sources may be used for the production of biochemicals. The model developed in this work has been used to predict the yields of 20 amino acids on such substrates and compare the yields obtained to the corresponding yields from glucose. It is well known that in cellular growth processes, part of the substrate is used for biomass production and part for maintenance. This means that one can distinguish between growth-related dissipation of Gibbs energy, $(D_s/r_x)_{gr}$, expressed kJ per C-mol produced biomass, where D_s is the dissipation of Gibbs energy, r_x is the biomass yield and the subscript *gr* refers to growth and maintenance related dissipation, m_e, expressed in kJ per hour per C-mol biomass present.

It has been found that the growth related dissipation mainly depends on the C-source used. The characteristics of growth-related dissipation in heterotrophic growth in *E. coli* are given below:

1. It is not very different for various electron acceptors.
2. It increases for a C-source with a smaller number of C-atoms. For example, glucose (6 C-atoms) requires much less dissipation than lactate (3 C-atoms).
3. It increases when the degree of reduction (γ_s) of the C-source deviates from about 4. A more reduced (e.g., CH_4 with γ_s = 8) or a more oxidized (e.g., formate, γ_s = 2) C-source would lead to higher dissipation values.

It can be seen from Table 7 that glucose has the lowest Gibbs-energy dissipation (i.e., it is the ideal substrate for growth). Citrate is a C-6 compound but has the largest Gibbs-energy dissipation and hence, growth on citrate should result in a lower biomass/amino acid yield than, for example, glucose. Glycerol is more reduced than glucose, but is a C-3 compound; and lactate is as reduced as glucose, but is a C-3 compound and, as with glycerol, energy must be expended in gluconeogenesis. No energy is needed for transport of glycerol and although glucose is taken up by a phosphotransferase system, there is no net energy loss. In contrast, the uptake of lactate is an energy-consuming process.

Table 8
Maximum Theoretical Yields of Amino Acids on Various Substrates

Compound	Yield (g/g substrate)			
	Lactate	Glycerol	Glucose	Citrate
Alanine	0.921	0.967	0.989	0.464
Arginine	0.636	0.813	0.748	0.506
Asparagine	0.978	1.294	1.144	0.688
Aspartate	1.150	1.446	1.342	0.693
Cysteine	0.542	0.726	0.655	0.424
Glutamate	0.817	0.799	0.817	0.766
Glutamine	0.811	0.793	0.811	0.705
Glycine	0.833	0.815	0.833	0.391
Histidine	0.532	0.713	0.643	0.373
Isoleucine	0.451	0.580	0.534	0.341
Leucine	0.485	0.474	0.485	0.227
Lysine	0.540	0.690	0.636	0.380
Methionine	0.401	0.533	0.480	0.319
Phenylalanine	0.409	0.538	0.485	0.258
Proline	0.546	0.620	0.633	0.446
Serine	1.016	1.141	1.167	0.547
Threonine	0.686	0.903	0.811	0.558
Tryptophan	0.392	0.526	0.469	0.266
Tyrosine	0.464	0.590	0.511	0.283
Valine	0.605	0.636	0.650	0.325
Biomass	0.444	0.589	0.527	0.367

The substrate uptake rate is based on 60 mmol of carbon atoms·g^{-1} DW·h^{-1}, i.e., 10 mmol Glc·g^{-1} DW·h^{-1} if the substrate is glucose (*Glc*) and 20 mmol GL·g^{-1} DW·h^{-1} if the substrate is glycerol (*GL*). The results from computations of the maximum theoretical yields for the various substrates are shown in Table 8. From this table, it can be easily seen that glucose and glycerol are the best substrates, from the energetic point of view, for the production of the amino acids.

Lactate as the Carbon Source

The results from Table 8 show that amino acid yields using lactate as the sole carbon source are lower than those using glucose. The reasons for the lower yields are straight forward. Biomass is built from C_4-C_5 central building blocks with an average γ_s of 4. If the molecular structure of the carbon source differs substantially from these central building blocks, as in the case of citrate, then a large number of reactions (carbon-carbon coupling; oxidation; reduction) must be performed in the primary pathways to convert the C-source to the building blocks. On the other hand, lesser number of reactions/modifications would be required if one uses C-sources which closely resemble the building blocks, e.g., glucose.

Glycerol as the Carbon Source

The yields of amino acids on glycerol have been found to be comparable to those based on glucose. Yields for the glutamate and serine family of amino acids have been found to be higher. Theoretically, glycerol, being a smaller molecule than glucose (3-carbon compared to 6-carbon) should require more energy for amino acid/biomass formation. Hence, growth on glycerol should result in a lower yield than glucose. The high yields of amino acids obtained with glycerol as the substrate is due to the fact that glycerol incorporation into the central metabolic pathways produces *NADH*.

$$GL + ATP \rightarrow GL3P + ADP \qquad \text{(Reac. No. 120)}$$

$$GL3P \rightarrow T3P + \mathbf{NADH} \qquad \text{(Reac. No. 121)}$$

NADH is easily converted to *ATP* in the electron transport chain. This results in a greater amount of *ATP* available for amino acid/biomass formation.

Citrate as the Carbon Source

Amino acid yields have been found to be fairly low for growth on citrate and it may be easily concluded that citrate should not be used as a substrate for the production of amino acids. The reason for the low yield is that citrate enters the metabolic system via the TCA cycle where a lot of carbon is lost in the form of carbon dioxide in the TCA cycle.

In addition, the deviation of the degree of reduction of citrate (3.0) from 4.0 increases the Gibbs-energy dissipation, resulting in a smaller amount of energy available for amino acid production.

The effect of cell growth rate on the yields of six amino acids from different C-sources has also investigated and the results are presented in Fig. 13. These amino acids were chosen because they are representative of the twenty amino acids that are produced in *E. coli* (i.e., they are located at different parts of the metabolic network). The different amino acid yields obtained with different C-sources may be attributed to whether carbon has to be oxidized to provide the required redox and energy. For *Ala, Gln,* and *Ser,* the decrease in amino acid production was observed to be slower at low cell growth rates compared to high cell growth rates, resulting in some sort of "switch point". For example, in *Ser* and *Ala* production, the switch point seems to occur at a cell growth rate of 0.5 h^{-1} whereas for *Gln*, it is 0.7 h^{-1}.

FLUX MAPS

Metabolic flux maps for *E. coli* growing on different C-sources and producing one of the above mentioned amino acids are shown in Figs. 14 to 19. The flux maps vary according to the point of entry of the substrate

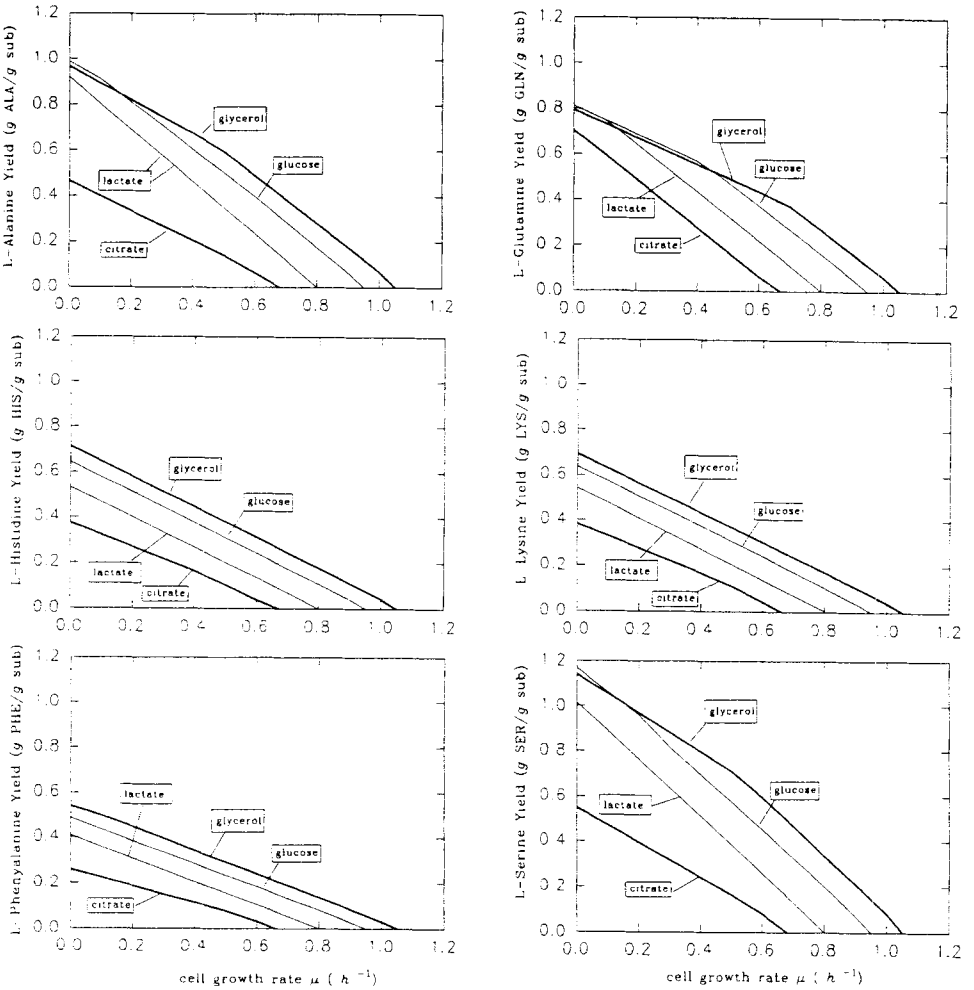

Fig. 13. Yields of various amino acids on citrate, glycerol, glucose and lactate.

and the reactions involved in the production of that particular amino acid. The flux maps are different even though the amino acid produced is the same. The model is able to utilize the shortest and least "expensive" (in terms of *ATP* consumption and loss of carbon as carbon dioxide) route for the formation of the amino acid.

Production of *Ala*

Several differences are observed in the flux maps for the production of *Ala* from different C-sources (Fig. 14). For glycerol and glucose, the TCA cycle is not activated. However, the TCA cycle is activated when lactate and citrate are used as substrates. In the case of lactate, the TCA cycle is activated because of the need for *NADH* for lactate to be incorporated into the central metabolic pathways.

$$\text{Pyr} + \text{NADH} \rightarrow \text{Lac} \qquad \text{(Reac. No. 30)}$$

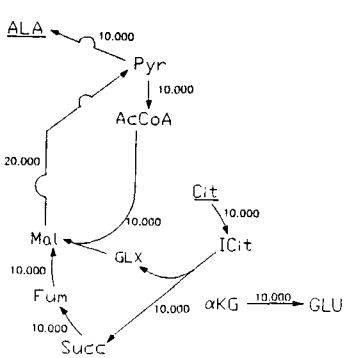

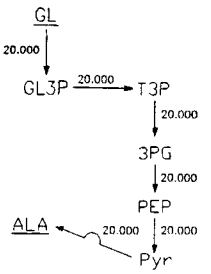

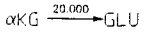

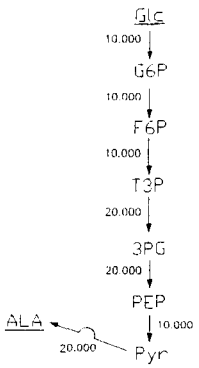

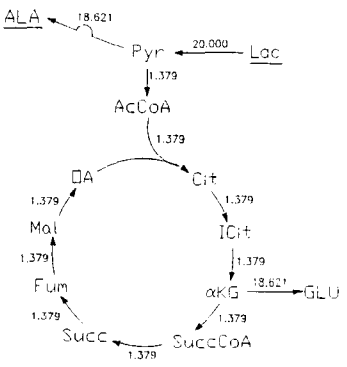

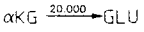

Fig. 14. Flux distribution maps of *E. coli* for the production of alanine (*Ala*) at $\mu = 0\ h^{-1}$ on substrates citrate (*Cit*), glycerol (*GL*), glucose (*Glc*), and lactate (*Lac*).

This requirement of *NADH* means that part of the substrate has to be oxidized to produce the required redox energy. Hence, the yield of *Ala* is low when lactate is the substrate. It is also observed that the flux from *αKG* to *Glu* (Reaction No. 78: $\alpha KG + NH_3 + NADPH \rightarrow Glu$) is exactly the same as the flux from *Pyr* to *Ala* (Reaction No. 88: $Pyr + Glu \rightarrow \alpha KG + Ala$). This is because *Glu* provides the necessary amino group to enable the production of *Ala*.

In the case of citrate, the TCA cycle is activated because it is part of the TCA cycle and there is no direct route for the conversion of citrate to *Ala*. Even then, only part of the TCA cycle (relevant reactions) appears to be activated.

Production of *Gln*

The metabolic maps for the production of *Gln* (Fig. 15) using glucose, lactate, and glycerol are almost identical and result in the same yields (0.833 C-Mol *Gln*/C-mol substrate). In general, the lower amino acid yields obtained when citrate is used as the substrate can be attributed to the loss of carbon dioxide in the reactions that lead from citrate to the various amino acids. For example, carbon is lost as carbon dioxide in the following four reactions in *Gln* production based on citrate.

$$\text{Pyr} \rightarrow \text{AcCoA} + \mathbf{Co_2} + \text{NADH} \qquad \text{(Reac. No. 13)}$$

$$\text{Mal} \rightarrow \text{Pyr} + \text{NADH} + \mathbf{CO_2} \qquad \text{(Reac. No. 29)}$$

$$\text{ICit} \rightarrow \alpha\text{KG} + \mathbf{CO_2} + \text{NADPH} \qquad \text{(Reac. No. 39)}$$

$$\alpha\text{KG} \rightarrow \text{SuccCoA} + \text{NADH} + \mathbf{CO_2} \qquad \text{(Reac. No. 41)}$$

Production of *His*

One common feature amongst the metabolic maps for the production of *His* is the activation of the *PPS* (Fig. 16). Production of *His* requires *ATP* (Reaction No. 93). *ATP* may be provided by the activation of the TCA cycle which is not activated when glycerol is the substrate. This is because the incorporation of glycerol into the central metabolic pathway provides *NADH* which can be subsequently oxidized in the electron transport system to give *ATP*. Another interesting point is that the flux linking *Glu* to *Gln* has the same value as the flux leading to *His* production (Reaction No. 93). This is because *Gln* is needed to provide the amino group in the biosynthesis of *His*.

$$\text{PRPP} + \mathbf{Gln} + \text{ATP} \rightarrow \text{His} + \text{PRAIC} + \alpha\text{KG} + 2\text{PPi} + 2\text{NADH} + \text{Pi} \qquad \text{(Reac. No. 93)}$$

One unique feature among the flux maps of *His* is the reactions leading from *Fum* to *Asp* in the TCA cycle. *Asp* is consumed in Reaction No. 96 while *Fum* is produced as a by-product. *Fum* is, in turn, converted back to *Asp* via the TCA cycle. The reason for the activation of these reactions is that *NADH* is generated in the process (Reaction No. 47). The use of this cycle from *Asp* to *Fum* produces the required *ATP* from the oxidation of *NADH* in the electron transport system. Moreover, this reduces the load on the TCA cycle and hence also reduces the loss of carbon in the form of carbon dioxide.

$$\mathbf{Fum} \rightarrow \text{Mal} \qquad \text{(Reac. No. 45)}$$

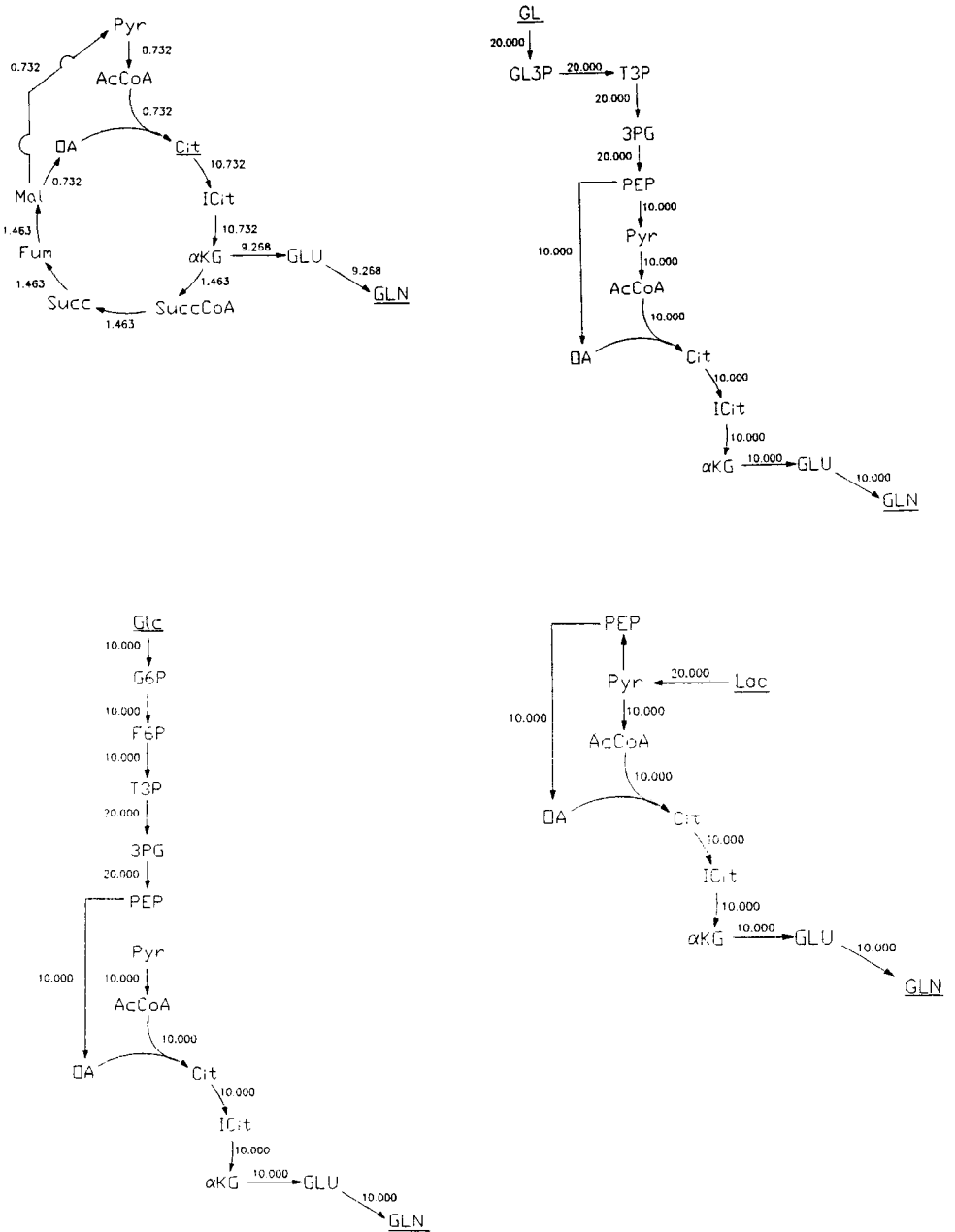

Fig. 15. Flux distribution maps of *E. coli* for the production of glutamine (*Glu*) at $\mu = 0\ h^{-1}$ on substrates citrate (*Cit*), glycerol (*GL*), glucose (*Glc*), and lactate (*Lac*).

$$\text{Mal} \rightarrow \text{OA } \mathbf{NADH} \qquad \text{(Reac. No. 47)}$$

$$\text{OA} + \text{Glu} \rightarrow \mathbf{Asp} + \alpha\text{KG} \qquad \text{(Reac. No. 69)}$$

$$\text{IMP} + \mathbf{Asp} + \text{GTP} \rightarrow \text{AMP} + \mathbf{Fum} + \text{GDP} + \text{Pi} \qquad \text{(Reac. No. 96)}$$

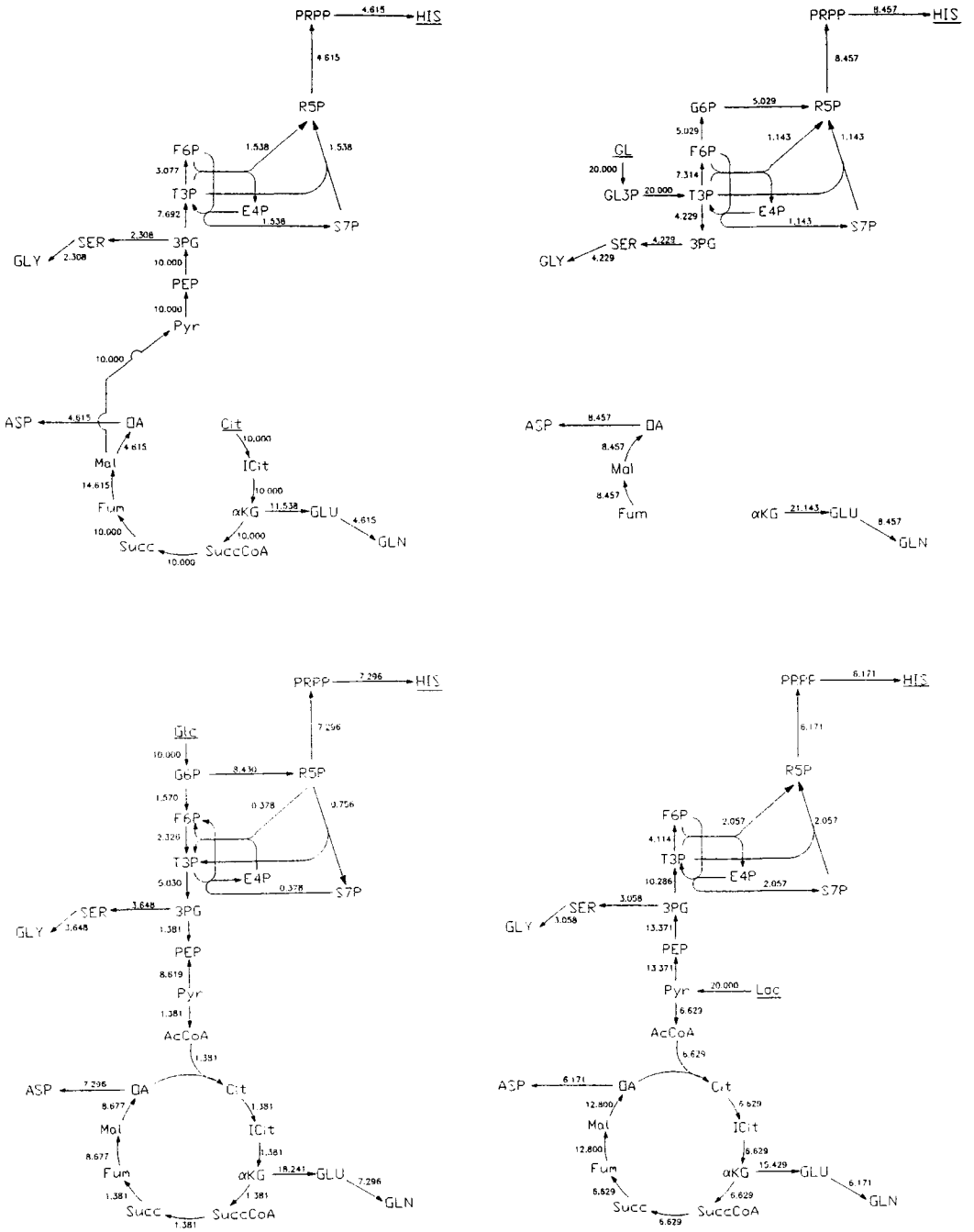

Fig. 16. Flux distribution maps of *E. coli* for the production of histidine (*His*) at $\mu = 0\ h^{-1}$ on substrates citrate (*Cit*), glycerol (*GL*), glucose (*Glc*), and lactate (*Lac*).

Production of *Lys*

As mentioned earlier, the production of *Lys* requires a large amount of *NADPH*. Different substrates employ different means of supplying *NADPH*. For glucose and glycerol, the pentose phosphate shunt appears

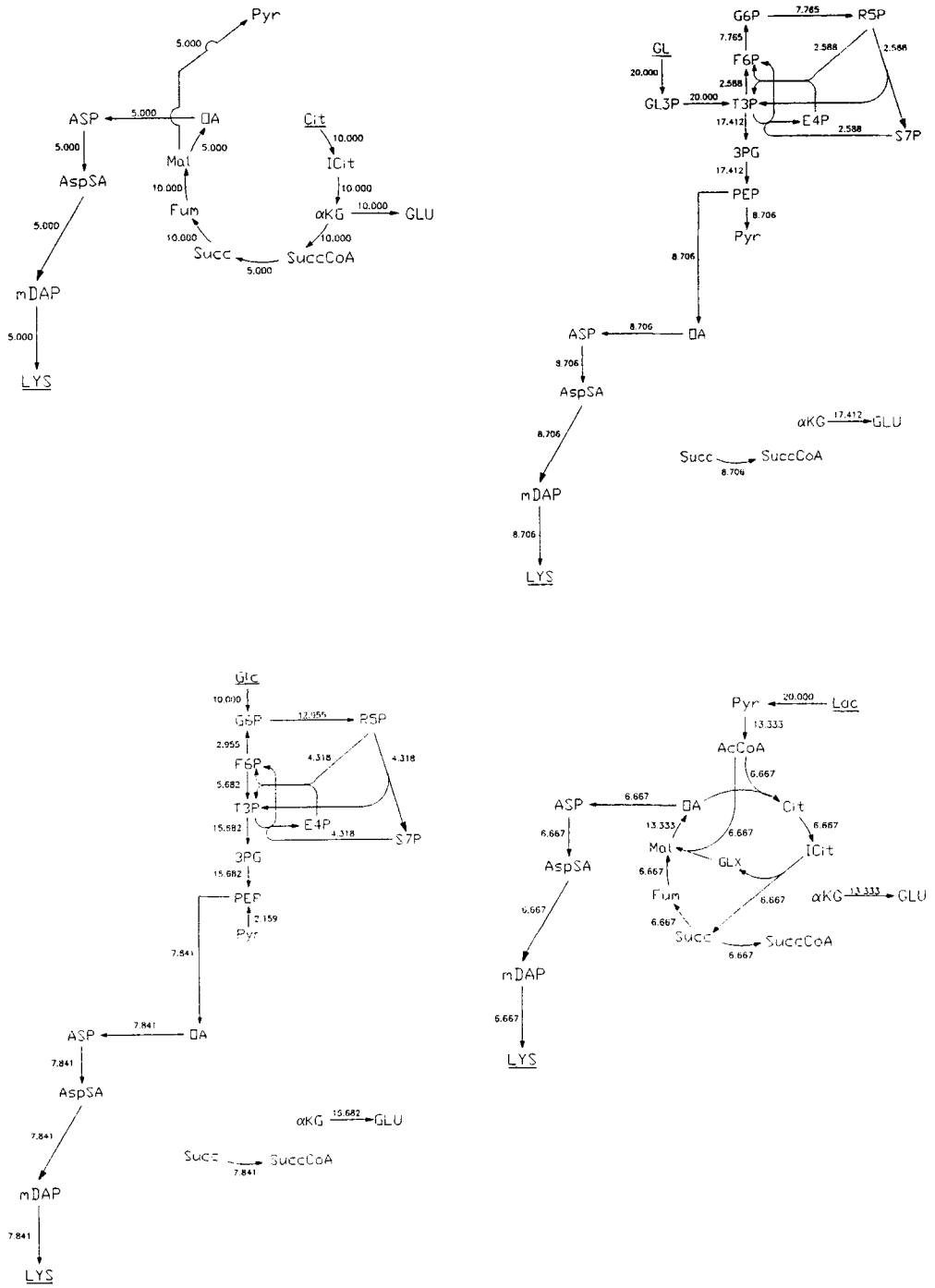

Fig. 17. Flux distribution maps of *E. coli* for the production of lysine (*Lys*) at $\mu = 0\ h^{-1}$ on substrates citrate (*Cit*), glycerol (*GL*), glucose (*Glc*), and lactate (*Lac*).

to be activated to supply the required *NADPH* (Fig. 17). For citrate, *NADPH* is supplied via the TCA cycle (Reaction No. 39) and the anaplerotic pathway (Reaction No. 28).

$$\text{Mal} \rightarrow \text{Pyr} + \mathbf{NADPH} + CO_2 \qquad \text{(Reac. No. 28)}$$

$$ICit \rightarrow \alpha KG + CO_2 + \mathbf{NADPH} \quad \text{(Reac. No. 39)}$$

As for lactate, *NADPH* is supplied from *NADH* in the electron transport system. *NADH* is being produced as a byproduct of Reaction Nos. 13 and 47.

$$Pyr \rightarrow AcCoA + CO_2 + \mathbf{NADH} \quad \text{(Reac. No. 13)}$$

$$Mal \rightarrow OA + \mathbf{NADH} \quad \text{(Reac. No. 47)}$$

Adequate *NADH* supplied via these routes are being converted to *NADPH* in the electron transport system such that Reaction No. 39 needs not be activated. Instead the glyoxylate shunt is being activated to avoid the loss of carbon in the form of carbon dioxide in Reaction No. 39.

Production of *Phe*

For the production of *Phe*, the TCA cycle has been activated for all three substrates except for glycerol (Fig. 18). This is due to the need to produce *NADH* which is subsequently oxidized in the electron transport system for the production of *ATP* which is required for *Phe* synthesis. On the other hand, the incorporation of glycerol into the central metabolic pathways produces the required *NADH* and hence reduces carbon losses, which resulted in relatively higher yields than other C-sources.

The fluxes of the reactions involved in the TCA cycle depend very much on whether the TCA cycle is also the supplier of *NADH* and *NADPH*. In the case of glucose, the TCA cycle is activated mainly for *ATP* production. The bulk of the required reducing power is supplied by the pentose phosphate shunt. This accounts for the low flux values in the TCA cycle. If the TCA cycle is the main source of *NADH*, *NADPH* and *ATP*, the fluxes tend to be large as in the case of citrate and lactate.

What is worth noting from the four flux maps in Fig. 18 is the branch linking *αKG* to *Glu* in the TCA cycle. This net flux has exactly the same value as the flux leading to *Phe*. This is because L-glutamate provides the necessary amino group which completes *Phe* formation.

$$2PEP + E4P + ATP + \mathbf{NADPH} \rightarrow Chor + ADP + 4Pi \quad \text{(Reac. No. 64)}$$

$$Chor + \mathbf{Glu} \rightarrow Phe + \alpha KG + CO_2 \quad \text{(Reac. No. 65)}$$

Another interesting point to note is the activation of the reaction: *G6P → R5P + CO₂ + 2NADPH* (Reac. No. 15) when glucose is the C-source. As with *Lys*, production of *Phe* requires *NADPH* and the supply of *NADPH* is met either by the activation of the *PPS* or via reactions: *Mal → Pyr + NADPH + CO₂* and *ICit → αKG + CO₂ + NADPH*.

Production of *Ser*

Metabolic maps for the production of *Ser* using various substrates appears to be very similar to that for the production of *Ala* (Fig. 19). This

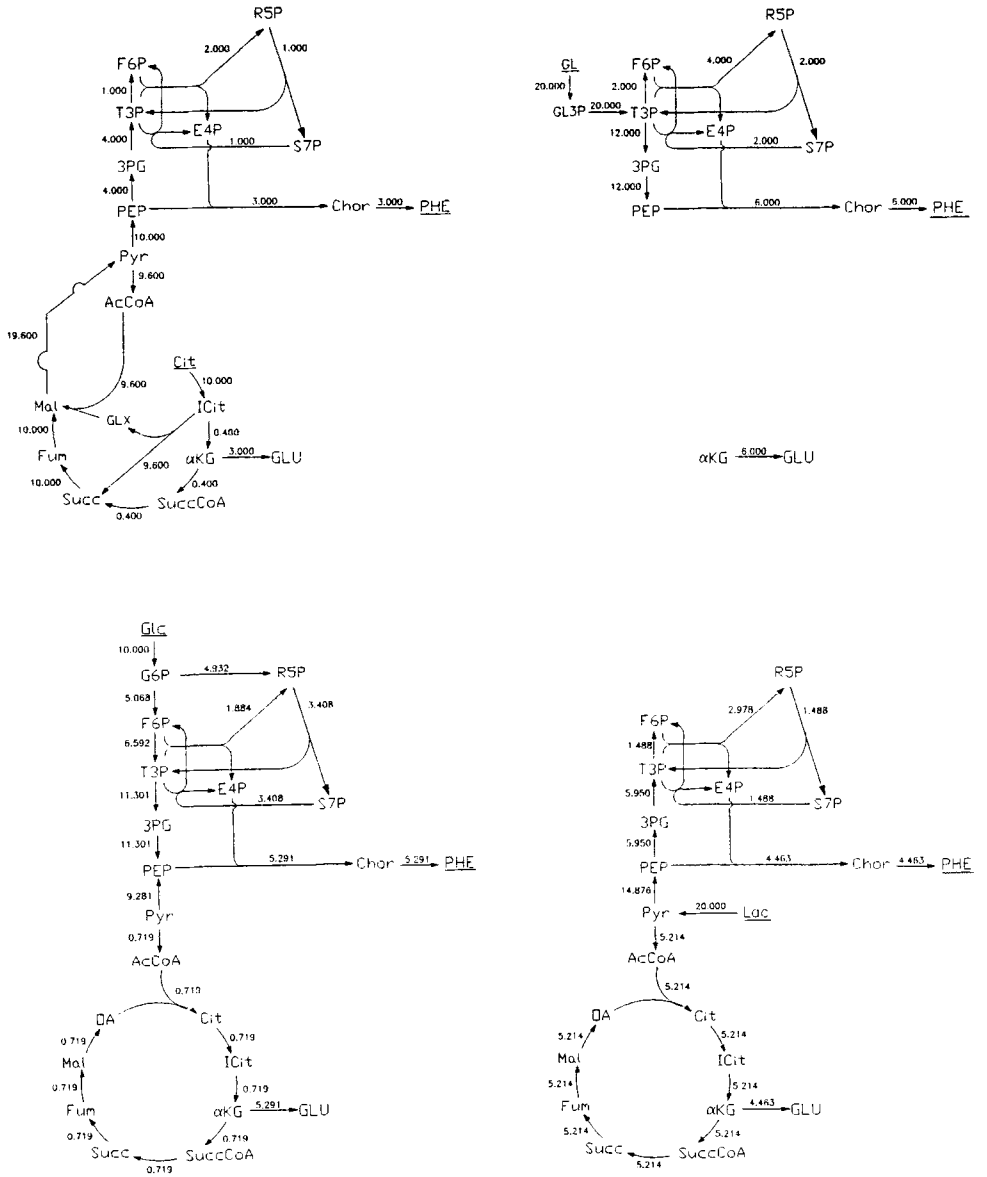

Fig. 18. Flux distribution maps of *E. coli* for the production of phenylalanine (*Phe*) at $\mu = 0\ h^{-1}$ on substrates citrate (*Cit*), glycerol (*GL*), glucose (*Glc*), and lactate (*Lac*).

is because similar reactions are involved in the production of these amino acids, resulting in similar yields.

One common feature in all metabolic maps involved in the production of the six amino acids is that the highest amino acid yields have been obtained for glycerol as the C-source. This is rather unusual since it is widely assumed that glucose is the ideal building block. In addition, glycerol has a higher Gibbs-energy dissipation compared to glucose which should result in correspondingly lower yields. However, as we have seen

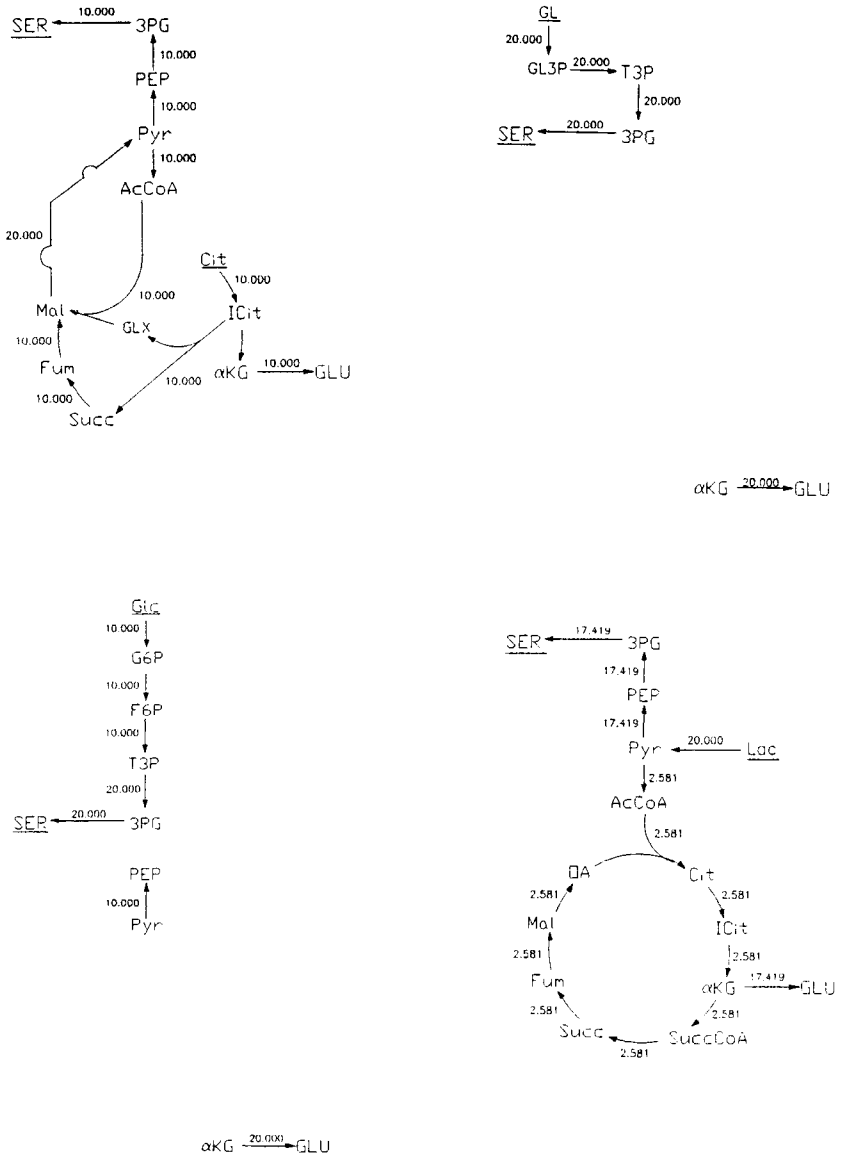

Fig. 19. Flux distribution maps of *E. coli* for the production of serine (*Ser*) at $\mu = 0\ h^{-1}$ on substrates citrate (*Cit*), glycerol (*GL*), glucose (*Glc*), and lactate (*Lac*).

from the metabolic maps, the increased yield can be attributed to the production of *NADH* during the incorporation of glycerol into the central metabolic pathways.

CONCLUSIONS

It has been demonstrated that the application of the mathematical programming formalism can be useful in identifying metabolic pathway

structures that should be capable of over-producing a metabolite of interest at a particular value of the cell growth rate. Such structures represent theoretical maxima and, as such, they may be unattainable in practice. However, the classification of the qualitative features of the optimal pathway structures and the identification of the ordered set of metabolic pathway regimes proposed in this work which should result in the overproduction of a particular metabolite over the complete range of cell growth rates, should provide useful targets for metabolic engineering research.

It should be considered that the above conclusions have been arrived at by using, solely, stoichiometric information on the metabolic pathways of *E. coli*. Although such stoichiometric constraints appear to delineate the solution space considerably, there are still substantial disparities between theoretical and experimental data. This could be attributed to a number of factors, such as the existence of mass transport limitations at the cell level and the fact that no reaction kinetic information has been incorporated into this model which, in addition, has not considered in any great detail the metabolic pathways involved in nitrogen assimilation. Finally, an experimental appraisal of the theoretical flux distributions presented here should complete the picture and improve our understanding of the metabolism of the *E. coli* cell.

APPENDIX A

A.1. The Reactions of the Model

I. Glycolysis and Gluconeogenesis

$$Glc + PEP \rightarrow Pyr + G6P \quad (1)$$
$$G6P \rightarrow F6P \quad (2)$$
$$F6P \rightarrow G6P \quad (3)$$
$$F6P + ATP \rightarrow 2\,T3P + ADP \quad (4)$$
$$2T3P \rightarrow F6P \quad (5)$$
$$T3P + ADP + Pi \rightarrow 3PG + ATP + NADH \quad (6)$$
$$3PG + ATP + NADH \rightarrow T3P + ADP + Pi \quad (7)$$
$$3PG \rightarrow PEP \quad (8)$$
$$PEP \rightarrow 3PG \quad (9)$$
$$PEP + ADP \rightarrow Pyr + ATP \quad (10)$$
$$Pyr + 2\,ATP \rightarrow PEP + 2ADP + Pi \quad (11)$$
$$Pyr \rightarrow AcCoA + Form \quad (12)$$
$$Pyr \rightarrow AcCoA + CO_2 + NADH \quad (13)$$
$$AcCoA + Form \rightarrow Pyr \quad (14)$$

II. Pentose Phosphate Shunt

$$G6P \rightarrow R5P + CO_2 + 2\,NADPH \quad (15)$$
$$R5P \rightarrow Xyl5P \quad (16)$$
$$Xyl5P \rightarrow R5P \quad (17)$$

R5P → Rib5P (18)
R5P → Rib5P (19)
2R5P → S7P + T3P (20)
S7P + T3P → 2R5P (21)
R5P + E4P → F6P + T3P (22)
F6P + T3P → R5P + E4P (23)
S7P + T3P → E4P + F6P (24)
E4P + F6P → S7P + T3P (25)

III. Anaplerotic Reactions

PEP + CO_2 → OA + Pi (26)
OA + ATP → PEP + CO_2 + ADP (27)
Mal → Pyr + NADPH + CO_2 (28)
Mal → Pyr + NADH + CO_2 (29)

IV. Branches from Glycolysis

Pyr + NADH → Lac (30)
Lac → Pyr + NADH (31)
AcCoA + ADP + Pi → Ac + ATP (32)
Ac + ATP → AcCoA + ADP + Pi (33)
Ac + ATP → AcCoA + PPi + AMP (34)
AcCoA + 2 NADH → Eth (35)

V. TCA-Cycle and Glyoxylate Shunt

OA + AcCoA → Cit (36)
Cit → ICit (37)
ICit → Cit (38)
ICit → αKG + CO_2 + NADPH (39)
αKG + CO_2 + NADPH → ICit (40)
αKG → SuccCoA + NADH + CO_2 (41)
SuccCoA + Pi + GDP → Succ + GTP (42)
Succ + GTP → SuccCoA + Pi + GDP (43)
Succ → Fum + $FADH_2$ (44)
Fum → Mal (45)
Mal → Fum (46)
Mal → OA + NADH (47)
ICit → GLX + Succ (48)
GLX + AcCoA → Mal (49)

VI. Electron Transport System

NADPH → NADH (50)
NADH + 2 Hexp → NADPH (51)
NADH → QH2 (52)
NADH → QH2 + 2 Hexp (53)
FADH → 2 Hexp (54)
Form → QH2 + Hexp + CO_2 (55)
QH2 → 2 Hexp (56)

ATP → 3 Hexp + ADP + Pi (57)
3 Hexp + ADP + Pi → ATP (58)

VII. Biosynthesis of Cofactors

DHF + NADPH → THF (59)
Gly + THF → MetTHF + CO_2 + NH_3 (60)
MetTHF + FADH → MTHF (61)
MetTHF → MeTHF + NADH (62)
MeTHF → FTHF (63)

VIII. Biosynthesis of Aromatic Amino Acids

2 PEP + E4P + ATP + NADPH → Chor + ADP + 4Pi (64)
Chor + Glu → Phe + αKG + CO_2 (65)
Chor + Glu → Tyr + αKG + NADH + CO_2 (66)
Chor + Gln + PRPP → IGP + Pyr + Glu + PPi + CO_2 (67)
IGP + Ser → T3P + Trp (68)

IX. Biosynthesis of Aspartate Family Amino Acids

OA + Glu → Asp + αKG (69)
Asp + Gln + ATP → Asn + Glu + AMP + PPi (70)
Asp + ATP + NADPH → ASPSA + ADP + Pi (71)
ASPSA + Pyr + Glu + SuccCoA + NADPH → mDAP + Succ + αKG (72)
mDAP → Lys + CO_2 (73)
ASPSA + NADPH → HSer (74)
HSer + Cys + SuccCoA + MTHF → Met + Pyr + Succ + NH_3 + THF (75)
HSer + ATP → Thr + ADP + Pi (76)
Thr + Glu + Pyr + NADPH → Ile + αKG + NH_3 + CO_2 (77)

X. Biosynthesis of Glutamate Family Amino Acids

αKG + NH_3 + NADPH → Glu (78)
Glu + ATP + NH_3 → Gln + ADP + Pi (79)
αKG + Gln + NADPH → 2 Glu (80)
Glu + ATP + 2 NADPH → Pro + ADP + Pi (81)
2 Glu + AcCoA + ATP + NADPH → Orn + Ac + αKG + ADP + Pi (82)
Orn + CaP → Citr + Pi (83)
Citr + Asp + ATP → Arg + Fum + AMP + PPi (84)

XI. Biosynthesis of Serine Family Amino Acids

3PG + Glu → Ser + αKG + NADH + Pi (85)
Ser + THF → Gly + MetTHF (86)
Ser + AcCoA + H_2S → Cys + Ac (87)

XII. Biosynthesis of Alanine Family Amino Acids

Pyr + Glu → αKG + Ala (88)
2 Pyr + NADPH → Kval + CO_2 (89)

Kval + Glu → αKG + Val (90)
Kval + AcCoA + Glu → Leu + αKG + NADH + CO_2 (91)

XIII. Biosynthesis of Histidine

R5P + ATP → PRPP + AMP (92)
PRPP + Gln + ATP → His + PRAIC + αKG + 2 PPi + 2 NADH + Pi (93)

XIV. Biosynthesis of Nucleotides

PRPP + 2 Gln + Gly + Asp + 4 ATP + CO_2 → (94)
PRAIC + 2 Glu + Fum + 4 ADP + 4 Pi + PPi + THF
PRAIC + FTHF → IMP + THF (95)
IMP + Asp + GTP → AMP + Fum + GDP + Pi (96)
IMP + Gln + ATP → GMP + Glu + NADH + AMP + PPi (97)
CaP + Asp + PRPP → UMP + NADH + PPi + Pi + CO_2 (98)
UTP + ATP + Gln → CTP + Glu + ADP + Pi (99)
ATP + AMP → 2 ADP (100)
ATP + GMP → ADP + GDP (101)
ATP + UMP → ADP + UDP (102)
ATP + CMP → ADP + CDP (103)
ATP + GDP → ADP + GTP (104)
GTP + ADP → GDP + ATP (105)
UDP + ATP → UTP + ADP (106)
CDP + ATP → CTP + ADP (107)
CTP → CDP + Pi (108)
ADP + TREDH → dADP + TRED (109)
GDP + TREDH → dGDP + TRED (110)
CDP + TREDH → dCDP + TRED (111)
UDP + TREDH → dUDP + TRED (112)
dADP + ATP → dATP + ADP (113)
dGDP + ATP → dGTP + ADP (114)
dCDP + ATP → dCTP + ADP (115)
dUDP + ATP → dUTP + ADP (116)
dUTP + MetTHF + 2ATP → dTTP + DHF + 2 ADP + PPi (117)
dCTP → dUTP + NH_3 (118)

XV. Reduction of Thioredoxin

TRED + NADPH → TREDH + NADP (119)

XVI. Biosynthesis of Fatty Acids and Phospholipids

GL + ATP → GL3P + ADP (120)
GL3P → T3P + NADH (121)
T3P + NADPH → GL3P (122)
AcCoA + ATP + CO_2 → MalACP + ADP + Pi (123)
AcCoA + 6 MalACP + 12 NADPH → C14:0 + 6CO_2 (124)
AcCoA + 6 MalACP + 11 NADPH → C14:1 + 6 CO_2 (125)
AcCoA + 7 MalACP + 14 NADPH → C16:0 + 7CO_2 (126)

$AcCoA + 7\,MalACP + 13\,NADPH \rightarrow C16{:}1 + 7CO_2$ (127)
$AcCoA + 8\,MalACP + 15\,NADPH \rightarrow C18{:}1 + 8CO_2$ (128)
$GL3P + C16{:}1 + C16{:}0 \rightarrow PA$ (129)
$PA + CTP \rightarrow CDPDG + PPi$ (130)
$CDPDG + Ser \rightarrow PS + CMP$ (131)
$PS \rightarrow PE + CO_2$ (132)
$CDPDG + GL3P \rightarrow PG + CMP + Pi$ (133)
$2\,PG \rightarrow CL + GL$ (134)
$Gln + ATP + CO_2 \rightarrow Glu + CaP + 2\,ADP + Pi$ (135)

XVII. Biomass Components

$F6P + Gln + AcCoA + UTP \rightarrow UDPNAG + Glu + PPi$ (136)
$3\,ADPHep + 2\,ADPGlc + 3\,CDPEtN + 3\,CMPKDO + 2\,UDPNAG + 2\,C14{:}0 + 4C14{:}1 + ATP \rightarrow LPS + 3\,CDP + 3\,CMP + UDP + UMP + 2\,Ac + 6\,ADP + PPi + 2\,Pi$ (137)
$2\,UDPNAG + 2\,Ala + mDAP + PEP + Glu + 5\,ATP + NADPH \rightarrow Peptide + UDP + UMP + 5\,ADP + 7\,Pi$ (138)
$R5P + PEP + CTP \rightarrow CMPKDO + PPi + 2\,Pi$ (139)
$Ser + CTP + ATP \rightarrow CDPEtN + ADP + PPi + CO_2$ (140)
$Orn \rightarrow PTRSC + CO_2$ (141)
$PTRSC + Met + 2\,ATP \rightarrow SPRMD + MetTHF + ADP + AMP + PPi + Pi + H_2S + CO_2$ (142)
$S7P + ATP \rightarrow ADPHep + PPi$ (143)
$G6P \rightarrow G1P$ (144)
$G1P \rightarrow G6P$ (145)
$G1P + ATP \rightarrow ADPGlc + PPi$ (146)
$ADPGlc + PPi \rightarrow G1P + ATP$ (147)

XVIII. Transport Reactions

$CO_2 \rightarrow$ exported (148)
imported $\rightarrow CO_2$ (149)
imported $\rightarrow NH_3$ (150)
$NH_3 \rightarrow$ exported (151)
$2ATP + 4\,NADPH \rightarrow AMP + ADP + H_2S + PPi + Pi$ (152)
$PPi \rightarrow 2\,Pi$ (153)
imported $\rightarrow$ Pi (154)
$Pi \rightarrow$ exported (155)

XIX. Biomass Formation

$45.13\,ATP + 0.58\,Gly + 0.04\,MTHF + 0.25\,Glu + 0.25\,Gln + 0.17\,Phe + 0.13\,Tyr + 0.2\,Ser + 0.05\,Trp + 0.22\,Asp + 0.22\,Asn + 0.32\,Lys + 0.06\,Cys + 0.14\,Met + 0.24\,Thr + 0.27\,Ile + 0.2\,Pro + 0.28\,Arg + 0.48\,Ala + 0.4\,Val + 0.42\,Leu + 0.06\,His + 0.2\,GTP + 0.13\,UTP + 0.12\,CTP + 0.02\,dATPB + 0.02\,dGTP + 0.02\,dCTP + 0.02\,dTTP + 0.09\,PE + 0.02\,PG + 0.02\,CL + 0.154\,ADPGlc + 0.01\,LPS + 0.02\,Peptide + 0.05PTRSC + 0.01\,SPRMD \rightarrow Biomass + 44.96\,ADP + ADP + 44.96\,Pi$ (156)

XX. THF Production

His → Glu + FTHF + NH_3 (157)
FTHF → MeTHF (158)
MeTHF → FNTHF (159)
FNTHF → Form + THF (160)
Form + THF + ATP → FNTHF + ADP + Pi (161)
FNTHF → THF + CO_2 (162)
MeTHF + NADH → MetTHF (163)

A.2. List of Abbreviations

Ac	Acetate
AcCoA	Acetyl coenzyme A
ADPGlc	ADP-Glucose
ADPHep	ADP-D-Glycerol-D-mannoheptose
ASPSA	Aspartate semihaldehyde
C14:0	Myristic acid (n-Tetradecanoic)
C14:1	β-Hydroxymyristic acid
C16:0	Palmitic acid (n-Hexadecanoic)
C16:1	Palmitoleic acid (hexa-9-decanoic)
C18:1	Oleic Acid
CaP	Carbamoyl-phosphate
CDP	Cytidine-5′-diphosphate
CDPDG	CDP-Diacylglycerol
CDPEtN	CDP-Ethanolamine
Chor	Chorismate
Cit	Citrate
Citr	Citrulline
CL	Diphosphatidylglycerol
CMP	Cytidine-5′-monophosphate
CMPKDO	CMP-3-Deoxy-D-manno-octulosonic acid
CO_2	Carbon dioxide
dADP	2′-Deoxy-adenosine-5′-diphosphate
dATP	2′-Deoxy-adenosine-5′-triphosphate
dCDP	2′-Deoxy-cytidine-5′-diphosphate
dCTP	2′-Deoxy-cytidine-5′-triphosphate
dGDP	2′-Deoxy-guanosine-5′-diphosphate
dGTP	2′-Deoxy-guanosine-5′-triphosphate
DHF	7,8-Dihydrofolate
dTTP	2′-Deoxy-thymidine-5′-triphosphate
dUDP	2′-Deoxy-uridine-5′-diphosphate
dUTP	2′-Deoxy-uridine-5′-triphosphate
E4P	Erythrose-4-phosphate
Eth	Ethanol
F6P	Fructose-6-phosphate
FADH	Flavine adenine dinucleotide (reduced)

Form	Formate
FTHF	N^5-Formimino-tetrahydrofolate
FNTHF	N^{10}-Formyl-tetrahydrofolate
Fum	Fumarate
G1P	Glucose-1-phosphate
G6P	Glucose-6-phosphate
GDP	Guanosine-5′-diphosphate
GL	Glycerol
GL3P	Glycerol-3-phosphate
Glc	Glucose
H_2S	Hydrogen sulfide
Hexp	Protons exported
HSer	Homoserine
ICit	Isocitrate
IGP	Indoleglycerolphosphate
IMP	Inosinemonophosphate
Lac	Lactate
LPS	Lipopolysaccharide
αKG	α-Ketoglutarate
Kval	Ketoisovalerate
Mal	Malate
MalACP	Malonyl-ACP
mDAP	meso-Diaminopimelate
MeTHF	N^5, N^{10}-Methenyl-tetrahydrofolate
MetTHF	N^5, N^{10}-Methylene-tetrahydrofolate
MTHF	N^5-Methyl-tetrahydrofolate
NH_3	Ammonia
OA	Oxaloacetate
Orn	Ornithine
PA	Phosphatidic acid
PE	Phosphatidyl-ethanolamine
PEP	Phosphoenolpyruvate
PG	Phosphatidyl-glycerol
3PG	Glycerate-3-phosphate
Pi	Inorganic orthophosphate
PPi	Inorganic pyrophosphate
PRAIC	5′-Phosphoribosyl-4-carboxamide-5-aminoimidazole
ProCoA	Propionyl-CoA
PRPP	Phosphoribosylpyrophosphate
PS	Phosphatidyl-serine
PTRSC	Putrescine
Pyr	Pyruvate
Pyrroline	Δ^1-Pyrroline-5-carboxylate
QH2	Hydroquinone
R5P	Ribulose-5-phosphate
Rib5P	Ribose-5-phosphate

S7P	Sedoheptulose-7-phosphate
SPRMD	Spermidine
Succ	Succinate
SuccCoA	Succinyl coenzyme A
T3P	Triose-3-phosphate (for glyceraldehyde-3-P and dihydroxyacetone-P)
TREDH	Thioredoxin (reduced)
UDPNAG	UDP-N-Acetyl-glucosamine

REFERENCES

1. Ikeda, M. and Katsumata, R. (1992), Metabolic engineering to produce tyrosine or phenylalanine in a tryptophan-producing *Corynebacterium glutamicum*. *Appl. Environ. Microbiol.* **58,** 781–785.
2. Backman, K. C., O-Connor, M. J., Maruya, A., Rudd, E., McKay, D., Balakrishnan, R., Radjai, M., DiPasquantonio, V., Shoda, D., Hatch, R., and Venkatasubrubramanian, K. (1990), Genetic engineering of metabolic pathways applied to the production of phenylalanine. *Ann. NY Acad. Sci.* **589,** 16–24.
3. Ohta, K., Beall, D. S., Mejia, P. J., Shanmugam, K. T., and Ingram L. O. (1991a), Genetic improvement of *Escherichia coli* for ethano production: chrosomsomal integration of *Zymomonas mobilis* genes encoding pyruvate decarboxylase and alcohol dehydrogenase II. *Appl. Environ. Microbiol.* **57,** 893–900.
4. Ohta, K., Beall, D. S., Mejia, P. J., Shanmugam, K. T., and Ingram L. O. (1991b), Metabolic engineering of *Klebisiella oxytoca* M5A1 for ethanol production from xylose and glucose. *Appl. Environ. Metabol.* **57,** 2810–2815.
5. Cox, K. L., Fishman, S. E., Hershberger, C. L., and Seno, E. T. (1987), Construction of genetically engineered microorganism having improved antibiotic-producing ability. *Eur. Pat. Appl.* EP 238323 A2; *Chem. Abstr.* **108,** 54455u.
6. Chen, C. W., Lin, H.-F., Kuo, C. L., Tsai, H.-L., and Tsai, J. F. -Y. (1988), Cloning and expression of a DNA sequence conferring Cephamycin C production. *Biotechnology* **6,** 1222–1224.
7. Beckmann, R. J., Cox, K. L., Rao, R. N., Richardson, M. A., and Seno, T. T. (1992), Macrolide biosynthetic genes for use in stretomyces and other organisms. US Patent, 5,098,837.
8. Slater, S. C., Voige, W. H., and Dennis, D. E. (1988), Cloning and expression in *Escherichia coli* of the *Alcaligenes eutrophus* H16 poly-beta-hydroxybutyrate biosynthetic pathway. *J. Bacteriol.* **170,** 4431–4436.
9. Tsai, H.-J. and Sandine, W. E. (1987), Conjugal transfer of lactose-fermenting ability from *Streptococcus lactis* C2 to *Leuconostoc cremoris* CAF7 yields *Leuconostoc* that ferment lactose and produce diacetyl. *J. Ind. Microbiol.* **2,** 25–33.
10. Garfinkel, D., Garfinkel, L., Pring, M., Green, S. B., and Chance, B. (1970), Computer applications to biochemical kinetics. *Ann. Rev. Biochem.*, **39,** 473–498.
11. Heinrich, R., Rapoport, S. M., and Rapoport, T. A. (1977), Metabolic regulation and mathematical models. *Prog. Biophs. Mol. Biol.*, **32,** 1–82.

11a. Hirao, T., Nakano, T., Azuma, T., Sugimoto, M., and Nakanishi T. (1989), L-Lysine production in continuous culture of an L-lysine hyperproducing mutant of *Corynebacterium glutamicum*. *Appl. Microbiol. Biotechnol.* **32,** 269–273.

12. Shiraishi, F. and Savageau, M. (1992a), The Tricarboxylic Acid Cycle in *Dictyostelium discoideum*. I Formation of alterative kinetic representations. *J. Biol. Chem.* **267,** 22,912–22,918.

13. Shiraishi, F. and Savageau, M. (1992b), The Tricarboxylic Acid Cycle in *Dictyostelium discoideum*. II Evaluation of model consistency and robustness. *J. Biol. Chem.* **267,** 22,919–22,925.
14. Shiraishi, F. and Savageau, M. (1992c), The Tricarboxylic Acid Cycle in *Dictyostelium discoideum*. III Analysis of steady state and dynamic behavior. *J. Biol. Chem.* **267,** 22,926–22,933.
15. Shiraishi, F. and Savageau, M. (1992d), The Tricarboxylic Acid Cycle in *Dictyostelium discoideum*. IV Resolution of discrepancies between alternative methods of analysis. *J. Biol. Chem.* **267,** 22,934–22,943.
16. Shiraishi, F. and Savageau, M. (1993), The Tricarboxylic Acid Cycle in *Dictyostelium discoideum*. V Systemic effects of including protein turnover in the current model. *J. Biol. Chem.* **268,** 16,917–16,928.
17. Fell, P. A. and Small, J. A. (1986), Fat synthesis in adipose tissue. An examination of stoichiometric constraints. *Biochem. J.* **238,** 781–786.
18. Majewski, R. A. and Domach, M. M. (1990), Simple constrained-optimization view of acetate overflow in *E. coli*. *Biotech. Bioeng.* **35,** 732–738.
19. Papoutsakis, E. T. (1984), Equations and calculations for fermentation of butyric acid bacteria. *Biotechnol. Bioeng.* **26,** 174–187.
20. Papoutsakis, E. T. and Meyer, C. L. (1985a), Equations and calculations of product yields and preferred pathways for butanediol and mixed-acid fermentations. *Biotechnol. Bioeng.* **27,** 50–66.
21. Papoutsakis, E. T. and Meyer, C. L. (1985b), Fermentations equations for propionic-acid bacteria and production of assorted oxychemicals from various chemicals. *Biotechnol. Bioeng.* **27,** 67–80.
21a. Satiawihardja, B., Cail, R. G., and Rogers, P. L. (1993), Kinetic analysis of L-lysine production by a fluoropyruvate sensitive mutant of *B. lactofermentum*. *Biotechnol. Letts.* **15,** 577–582.
22. Tsai, S. P. and Lee, Y. H. (1988), Application of Gibbs' rule and a simple pathway method to microbial stoichiometry. *Biotechnol. Prog.* **4(2),** 82–88.
23. Noorman, H. J., Heijnen, J. J., Luyben, K. Ch. A. M. (1991), Linear relations in microbial reaction systems: A general overview of their origin, form and use. *Biotechnol. Bioeng.* **38,** 603–618.
24. Oh, N. S. and Sernetz, M. (1993), Turnover characteristics in continuous L-lysine fermentation. *Appl. Microbiol. Biotechnol.* **39,** 691–695.
25. Savinell, J. M. and Palsson, B. O. (1992a), Network analysis of intermediary metabolism using linear optimization: I. Development of mathematical formalism. *J. Theor. Biol.* **154,** 421–454.
26. Savinell, J. M. and Palsson, B. O. (1992b), Network analysis of intermediary metabolism using linear optimization: II. Interpretation of hybridoma cell metabolism. *J. Theor. Biol.* **154,** 455–473.
27. Varma, A. and Palsson, B. O. (1993), Metabolic capabilities of *Escherichia coli*. I. Synthesis of Biosynthetic Precursors and Cofactors. *J. Theor. Biol.* **165,** 477–502.
28. Varma, A., Boesch, B. W., and Palsson, B. O. (1993a), Biochemical production capabilities of *Escherichia coli*. *Biotechnol. Bioeng.* **42,** 59–73.
29. Varma, A., Boesch, B. W., and Palsson, B. O. (1993b), Stoichiometric interpretation of *Escherichia coli* glucose catabolism under various oxygenation rates. *Appl. Environ. Microbiol.* **59,** 2465–2473.
30. Stephanopoulos, G. and Vallino, J. J. (1991), Network rigidity and metabolic engineering in metabolite overproduction. *Science,* **252,** 1675–1681.
31. Kiss, R. D. and Stephanopoulos, G. (1991), Metabolic characterization of a L-lysine-producing strain by continuous culture. *Biotechnol. Bioeng.* **39,** 565–574.
32. Schaechter, Maaloe, E. O., and Kjeldgaard, N. O. (1958), Dependence on medium temperature of cell size and chemical composition during balanced growth of *Salmonella typhimurium*. *J. Gen. Microbiol.* **19,** 52–606.

33. Bremer, H. and Dennis, P. (1987), Modulation of chemical composition and other parameters of the cell by growth rate in *Escherichia coli* and *Salmonella typhimurium. Cellular and molecular biology*, Vol. 2, Neidhardt, F. C., ed. American Society for Microbiology, Washington, DC, pp. 1527–1542.
34. Churchward, G., Bremer, H., and Young, R. (1982), Macromolecular composition of bacteria. *J. Theor. Biol.* **94,** 651–670.
35. Cooper, S. and Helmstetter, C. (1981), Chromosome replication and the division cycle of *Escherichia coli. J. Bacteriol.* **145,** 1231–1238.
36. Schleif, R. (1967), Control of the production of ribosomal protein. *J. Mol. Biol.* **27,** 41–55.
37. Nielsen, J. and Villadsen, J. (1994), *Bioreaction engineering principles,* Plenum Press, New York, pp. 7–96.
38. Mathews, C. K. and van Holde, K. E. (1990), *Biochemistry,* Wokingham: The Benjamin/Cummings, Redwood City, pp. 696–698.
39. Park, N. H. and Rogers, P. L. (1985), L-Phenylalanine production in a continuous culture using a hyperproducing mutant of *Escherichia coli* K-12. *Chem. Eng. Commun.* **45,** 185–196.
40. Choi, Y. J. and Tribe, D. E. (1982), Continuous production of phenylalanine using an *Escherichia coli* regulatory mutant. *Biotechnol. Letts.* **4,** 223–228.
41. Chambost, J. P. and Fraenkel, D. G. (1980), The use of 6-^{14}C-labelled glucose to assess futile cycling in *Escherichia coli. J. Biol. Chem.* **255,** 2867–2869.
42. Daldal, F. and Raenkel, D. G. (1983), Assessment of a futile cycle involving reconversion of fructose-6-phosphate to fructose-1,6-biphosphate during gluconeogenic growth of *Escherichia coli. J. Bacteriol.* **153,** 390–394.
43. Tsuchida, T., Yoshinaga, F., Kubota, K., and Momose, H. (1975), Production of L-valine by 2-thiazolealanine resistant mutants derived from glutamic acid producing bacteria. *Agri. Biol. Chem.* **39,** 1319–1322.
44. Ingraham, J. L., Maaloe, O., and Neidhardt, C. (1983), *Growth of the bacterial cell.* Sunderland, Mass: Sinauer Associates, Inc.
45. Neidhardt, F. C., ed., (1987), *Escherichia coli and Salmonella typhimurium. Cellular and Molecular Biology,* Vol 1 and 2, American Society for Microbiology, Washington, DC.
46. Yoshihara, Y., Kawahara, Y., Tanaka, Y., and Ikeda, S. (1992), Method for producing L-amino acids by fermentation. US Patent No. 5,164,307.
47. Furukawa, S., Ozaki, A., Nakanishi, T., and Sugimoto, M. (1988b), Breeding of an L-isoleucine producer by protoplast fusion of *Corynebacterium glutamicum. Appl. Microbiol. Biotechnol.* **29,** 248–252.
48. Dunyak, S. A. and Cook, T. M. (1985), Continuous fermenter growth of a methionine-overproducing mutant of *Cadida utilis. Appl. Microbiol. Biotechnol.* **21,** 182–382.
49. Tanaka, T., Yamamoto, K., Towprayoon, S., Nakajima, H., Sonomoto, K., Yokozeki, K., Kubota, K., and Tanaka, A. (1989), Continuous production of serine by immobilized growing *Corynebacterium glycinophilum* cells. *Appl. Microbiol. Biotechnol.* **30,** 564–568.
50. Azuma, S., Tsunekawa, K., Okabe, M., Okamoto, R., and Aiba, S. (1993), Hyperproduction of L-tryptophan via fermentation with crystallization. *Appl. Microbiol. Biotechnol.* **39,** 471–476.